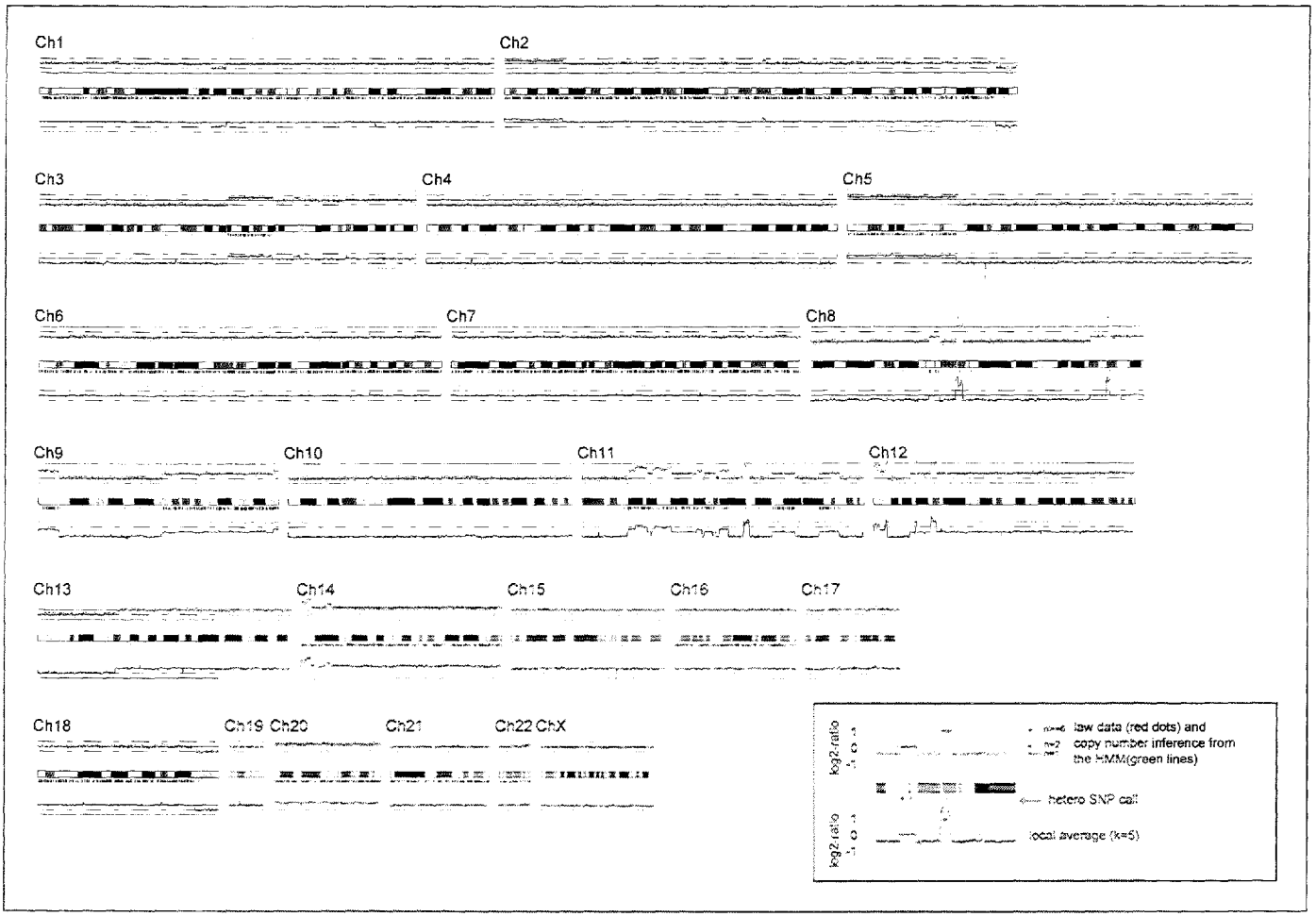

Figure 3. Analysis of CRL-5929 using five best-fit references and the whole genome result. *Red dots*, raw log 2-ratio values for each SNPs. Copy number inferences from a hidden Markov model (*green lines*) and local mean analysis for five consecutive SNPs (*blue curves*) are appended. Heterozygous SNP calls are marked with green bar lines beneath the chromosomes.

every combination of two arrays from 96 normal individuals (see Materials and Methods). This resulted in a considerable difference in SD values among different combinations of samples (Fig. 1*A* (*left*) and Supplementary Fig. 1). We hypothesized that different PCR kinetics among experiments could be the origin of these highly variable SD values and that adjusting for these experimental variables may allow for more accurate comparisons (Supplementary Methods). It should be noted from the block-like structures of the SD graph that the behavior of SD values is largely determined by the group of experiments done together, rather than the individual experiments.

To assess the dependence of the log 2 ratios of signals on PCR kinetics, we plotted log 2 ratios against several variables that may affect PCR reactions in different experiments, including length of PCR fragments and GC content (Fig. 1*B*). By compensating for the effects of these variables using two-step quadratic regressions, the log 2 ratios almost completely offset the dependencies of log 2 ratios on these variables and the SD value between the given two experiments is reduced from 0.88 to 0.40 (Fig. 1*B* and *C*). In fact, these compensation procedures dramatically improve the distribution of SD values among 96 normal samples, enabling comparisons across different samples or groups of experiments (Fig. 1*A*, *right*). SNPs located on fragments shorter than 500 bp, which account for 2.9% of total SNPs, tend to be resistant to these compensations and were precluded from the analyses altogether.

Optimization of reference selection. Although correcting for the fragment length and GC content dramatically reduces SD values, there was still considerable variation among different samples. Therefore, we explored the effects of using different reference sets. The type of reference set used largely depends on the following: (*a*) cases where tumor and normal DNA are available from the same patient (paired normal samples) and (*b*) cases where only the test or tumor sample is available. Use of a paired normal sample coupled with compensation for variability across experimental conditions generally gives lower SD values. However, the benefit of having a paired normal sample for a reference tends to be diminished when test and reference samples are processed separately (data not shown). The case when a paired normal sample for a reference is unavailable is more complicated. Although the array that shows the lowest SD value for the test sample is a candidate for the reference, we investigated choosing the average of multiple samples with the lowest SD values or best-fit samples as a reference.

To determine the effect of averaging multiple references on SD values, data from 96 normal samples were compared with the averages of varying numbers of the best-fit references, and SD values were calculated for each comparison (Fig. 1*D*). As the number of samples increases to five, the SD value gradually decreases to <0.15

for most normal samples and then reaches a plateau, suggesting that taking an average of at least five best-fit samples is sufficient to optimize the comparison (Fig. 2*A*).

A direct comparison of the copy number estimation using a paired normal reference and best-fit reference was also evaluated for a small cell carcinoma cell line (CRL-5929). The results using a paired normal reference show a slightly lower SD value (0.141 versus 0.177) and smaller fluctuations of baselines than with the best-fit multiple references (Supplementary Fig. 2*A*). However, copy number inference from the hidden Markov model (see Materials and Methods) analysis and local averaging gives an equivalent result (Supplementary Fig. 2*B*). This suggests that the multiple best-fit references are an excellent substitute in cases where a constitutional paired normal reference is not available.

Validation of new algorithm using normal and tumor samples. We evaluated the performance of this new algorithm by analyzing a variety of samples. Figure 2*B* shows a representative analysis of a glioma specimen, showing the dramatic reduction of baseline fluctuations or SD values when using this algorithm relative to raw log 2 ratios. The raw data (Fig. 2*B*-1) has an SD of 0.365, which is reduced to 0.222 after applying a single best-fit reference (Fig. 2*B*-2). A further improvement was seen when using multiple best-fit references, SD = 0.118 (Fig. 2*B*-3). Regions of homozygous and hemizygous deletion are indicated by small and large arrows, respectively. As tumor samples frequently exhibit complex chromosome abnormalities with extensive genetic imbalances (22), analysis of tumor specimens requires additional considerations in selection of references. SD values may be disproportionately inflated or overwhelmed by the effect of genetic abnormalities when all autosomal signals are included in the calculation of SD values. To circumvent this problem and to calculate proper SD values for reference selection, we adopted a two-step approach. We first made a tentative estimation of the copy number changes by using all autosomal signals and predicted the regions that are diploid by reference to other independent information (FISH, PCR, or results in the literature). In the second step, one of these diploid regions was used for normalization and for calculation of SD values to identify the best-fit references. This final step further improved the SD value, 0.114 (Fig. 2*B*-4).

Reductions of SD values in different tumor samples are summarized in Fig. 2*C*. The SD values from 33 tumor samples were calculated from raw data, as well as using the new algorithm with five best-fit references. The distribution of SD values is clearly decreased using the new algorithm. Figure 2*C* also illustrates the results using limited regional SNPs, local averaging of five or ten consecutive SNPs, and using a paired normal reference. After all corrections and optimizations of best-fit reference samples, a local mean procedure was applied which results in lower SD values relative to the paired normal reference sample, where no local mean was used. All of these analyses resulted in a dramatic reduction in the SD values relative to the raw data, which enables genome-wide copy number detection with a high degree of accuracy (Fig. 3).

Sensitivity of copy number analysis using improved algorithm. We evaluated the sensitivity of our copy number detection algorithm by calculating mean log 2 ratios for those regions having known copy number alterations. The observed

Table 1. Comprehensive list of homozygous deletions and gains in tumor cell lines

Sample*	Change	Length (kb)†	Cytoband	SNPs involved	Genes involved	Confirmation‡
CRL-5929	Deletion	5.5-76	5q13.1	4	*PIK3R1*	PCR (ID1)
	Gain	2,253-2,652	8q12.2-8q12.3	146	*ASPH*, *GGH*, others	FISH (RP11-234F8)
	Gain	1,347-1,475	8q24.21	83	*MYC*	FISH (RP11-145G10)
	Gain	1,662-1,771	11q14	113	*ME3*, *SYTL2*, others	FISH (RP11-90K17)
	Gain	566-627	12p13.33	23	*CACNA1C*, *DCP1B*, others	
	Gain	825-919	12p13.32	37	*CCND2*, *PARP11*	
	Gain	2,720-2,780	12p13.31	31	*LAG3*, *GAPD*, others	FISH (RP11-166G2)
	Gain	693-888	12p12.1	39	*SLCO1*, *IAPP*, others	
	Gain	1,925-2,090	12p11	115	*PTHLH*, *MRPS35*, others	FISH (RP11-74J4)
	Gain	609-648	14q11.2	48	*CCNB1IP1*	FISH (RP11-98N22)
	Gain	1,770-1,918	14q11.2	93	*SALL2*, *METTL3*, others	FISH (RP11-70F9)
	Deletion	0.9-29	15q23	3	—	PCR (ID2)
CRL5872	Gain	8,763-10,224	1q21.2-1q22	92	*BCL9*, *IL6R*, others	FISH (RP11-71L20)
	Gain	1,703-2,814	5p15.33	41	*IRX4*, *NDUFS6*	FISH (RP11-20B3)
	Gain	1,183-2,113	8p11.22-8p11.21	43	*INDO*, *ADAM2*	FISH (RP11-262I23)
	Deletion	54-131	9p23	9	—	PCR (ID4)
	Deletion	316-404	9p23	16	—	
	Deletion	391-556	9p22.3	14	*CER1*, *FREM1*	
	Deletion	1,498-1,684	9p22.2	42	*SH3GL2*	
	Deletion	1,237-1,457	9p21.3	44	*IFNA*, *CDKN2A*, others	PCR (ID5)

NOTE: Homozygous deletions ($n = 0$) and high grade gains ($n > 4$) were identified using a hidden Markov model.

*All samples are compared with paired normal references to distinguish between tumor-specific copy number alterations and copy number polymorphisms.

†Minimal size range is the distance of both ends of consecutive SNPs that meet the criteria. Maximal size range is the distance of the SNPs that flank the deleted or amplified regions. Based on UCSC Build 16 (hg16) assembly (http://genome.ucsc.edu/cgi-bin/hgGateway).

‡The probe names used in FISH analysis and the primer set IDs used in PCR analysis are shown in parentheses. See Supplementary Tables 1 and 2 for details.

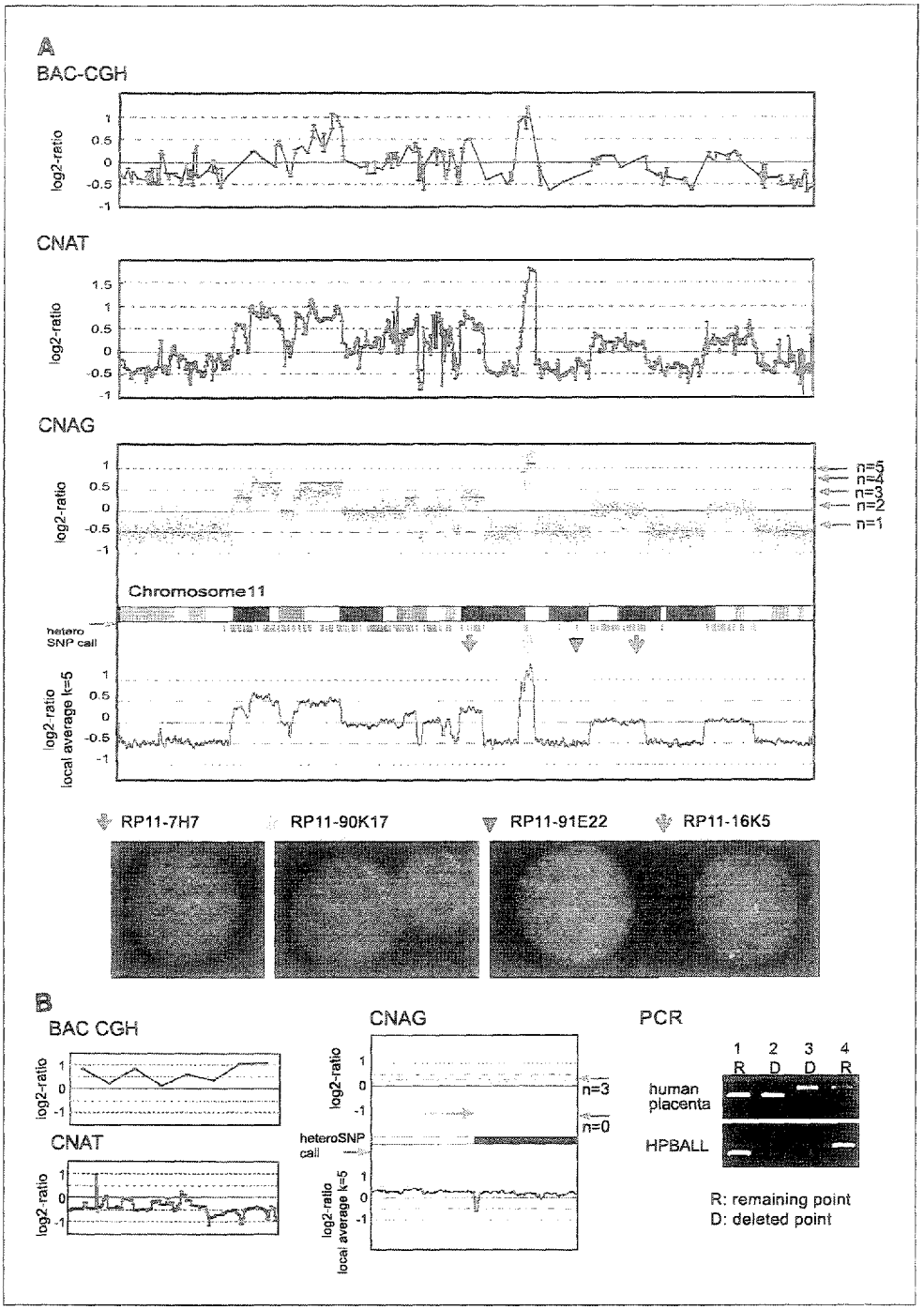

Figure 4. *A*, comparison of BAC array (*top*), CNAT (*middle*), and CNAG (*bottom*). CRL-5969 was used as paired normal reference in all methods. Chromosome 11 is represented. FISH analysis confirmed the detected changes. *B*, immature T-cell line HPB-ALL was examined using BAC-arrays (*left top*), CNAT (*left bottom*), and CNAG (*middle*). CNAG detected a homozygous deletion in 2p16.3 (*red arrow*, position 48,002,999-48,059,096) that was not detected by BAC-array or CNAT. The deletion was confirmed by PCR (*right*). 2p21-2p16.3 is presented for all three methods.

mean log 2 ratio for X chromosomes between 48 males and 48 females was −0.49 (SD = 0.035), which is about half of the expected value (= −1) for the single copy difference (Supplementary Fig. 3). Similarly, the observed mean log 2 ratio for known trisomy in CRL-5929 in chromosome 20[9] was 0.36, compared with the expected value of 0.585. These discrepancies are thought to result from nonspecific background hybridization, which could not be measured and subtracted before taking log 2 ratios, although the background factors can be theoretically estimated and used for performing copy number inference using a hidden Markov model (Supplementary Method). Because the SD value of log 2 ratios for baseline diploid SNPs is 0.18 ± 0.03 with best-fit references or lower with a paired normal reference, the estimated S/N ratio is ~2.0 (for trisomy) or more (for monosomy) in most cases.

Estimation of the resolution is directly proportional to the distribution of SNP markers. We determined the size of genomic alterations in CRL-5929 and CRL-5872 cell lines (Table 1). Deletions of less than 500 kb at 14q11.2 (T-cell receptor α) and less than 393 kb at 7q34 (T-cell receptor β) were observed in the immature T-cell line HPB-ALL; these were caused by a T-cell receptor rearrangement (23). The genomic regions comprising these deletions contain approximately 20 and 10 SNPs, respectively, from the Affymetrix GeneChip Mapping 100K arrays. As the number of SNP markers

[9] http://www.path.cam.ac.uk/~pawefish/LungCellLineDescriptions/NCI-H2171.html

increases, the accuracy of size determinations increases and even smaller deletions are likely to be detected.

Finally, we compared BAC-CGH arrays, CNAT, and CNAG. BAC-arrays containing 3,151 FISH-mapped BAC/PAC clones with an average resolution of 1.0 Mb were constructed. The CRL-5929 cell line was examined using the BAC-array (Fig. 4*A*, *top*), CNAT (Fig. 4*A*, *middle*), and CNAG (Fig. 4*A*, *bottom*). The resolution on the SNP array allows for much finer mapping than BAC arrays, and additional compensations applied in CNAG provide more distinct copy number detection than CNAT. FISH analysis showed complete concordance with this method (Fig. 4*A*, *bottom*). This is more clearly seen in the immature T-cell line (HPB-ALL) on chromosome 2 (Fig. 4*B*). In this case, a homozygous deletion in 2p16.3 (*red arrow*) was detected by the 100K SNP array (Fig. 4*B*, *right*) but not detected by the BAC-array or CNAT (Fig. 4*B* (*left*), *top* and *bottom*, respectively). Lack of PCR product designed within the deleted region in HPB-ALL verified the deletion (Fig. 4*B*, *right*).

Allele-based copy number analysis. Another potential benefit from using a paired normal reference is the allele-based copy number analysis. In this approach, copy number estimates are done separately for each of the heterozygous SNPs (Fig. 5). The ratios can be separately defined for each of the alleles, grouped together into the larger (red) and smaller (green) ones and plotted in chromosomal order (Fig. 5; see Materials and Method). Although the analysis is confined to only heterozygous SNPs (mean heterozygosity of the Affymetrix GeneChip Mapping 100K SNPs is 0.29), it can effectively unmask regions showing copy neutral LOH due to genetic imbalances (asterisks in Fig. 5, *middle*), which are not detected by non-allele-based analysis (Fig. 5, *top*) or conventional BAC-array CGH.

Discussion

Recently, synthesized oligonucleotide microarrays have been used as alternatives to conventional BAC-array CGH for genome-wide copy number analysis (8–15). Large numbers of SNP markers are expected to enable ultra high-resolution copy number analysis; however, currently available algorithms do not take into account variation across different experiments, which can result in low S/N and high SD values. To address this problem, we developed a novelalgorithm for Affymetrix GeneChip Mapping 100K arrays, which includes robust compensations for systematic deviations of raw signal ratios across different experimental conditions and optimizes selection of the best-fit references. Together, these features effectively reduce heterogeneity between experiments and improve the SD value of log 2 ratios from 0.67 ± 0.12 to 0.18 ± 0.03, which is considerably lower than values reported for

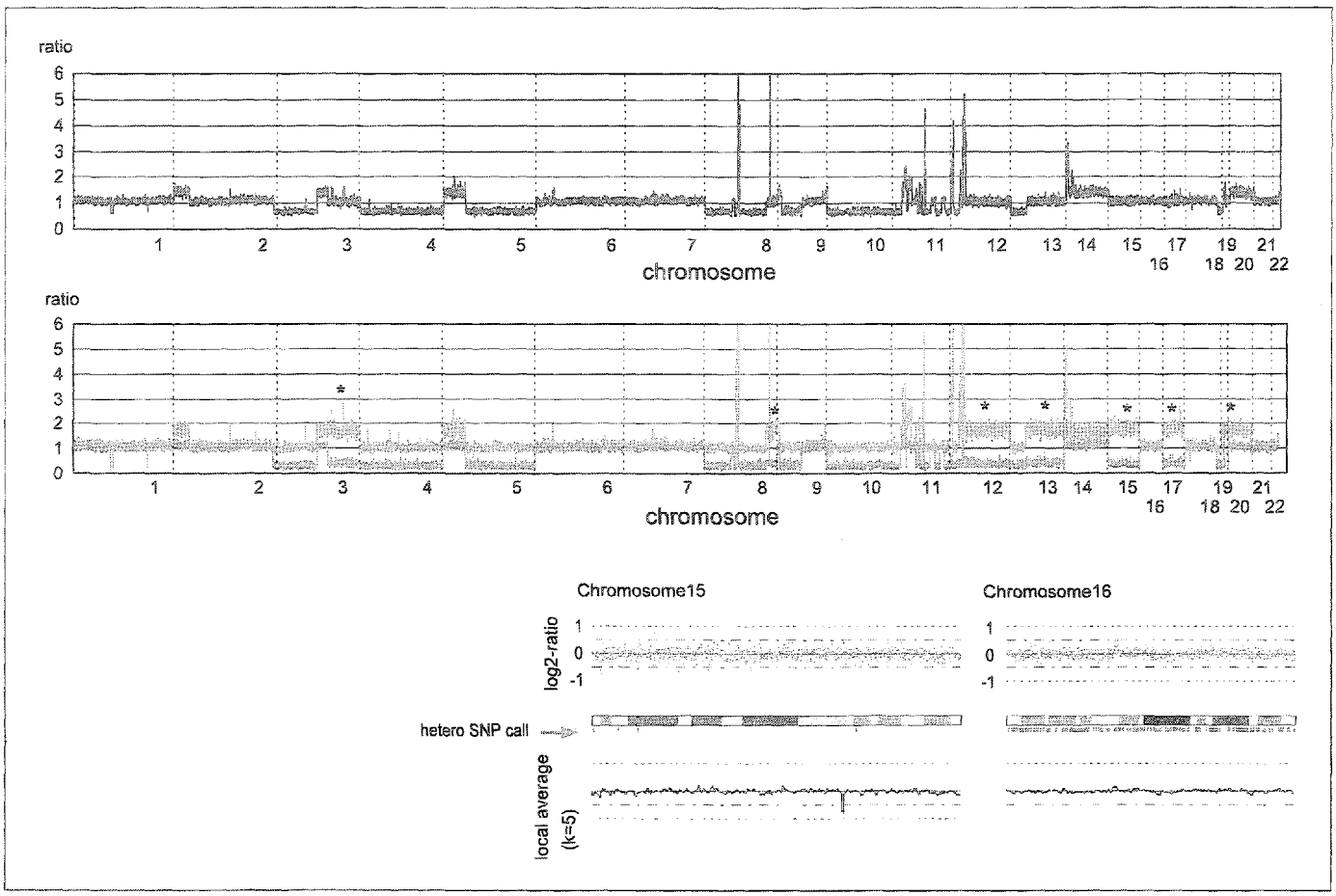

Figure 5. Copy number views of allele-based (*middle*) and non-allele-based analyses (*top* and *bottom*) of the same tumor samples as in Fig. 3 using the local mean analysis ($k = 5$). In the allele-based copy number view, the larger (A_{max}, *red lines*) and the smaller (A_{min}, *green lines*) log 2 ratios of the two log 2 ratios for allele A and allele B signals are separately grouped. Regions having copy neutral LOH as well as monosomy can be inferred from disappearance of heterozygous SNP calls in this non-allele-based analysis (*bottom*). Whereas no copy number changes are observed in both chromosomes 15 and 16, chromosome 15 shows copy neutral LOH as clearly seen in the allele-based copy number view (*middle*). Note that the existence of copy neutral LOH in chromosome 15 is inferred from the disappearance of heterozygous SNP calls in non-allele-based analysis (*bottom*).

oligonucleotide CGH-arrays (24). The SD value further decreases to 0.10 when log 2 ratios are locally averaged for consecutive five to ten SNPs (Fig. 2*C*). The reduction of SD values greatly contributes to high-quality copy number analysis across separately manipulated best-fit references.

Use of a paired normal reference further reduces SD values to 0.16 ± 0.03 ($P < 0.05$ for best-fit references), as comparison of signals is more accurately done between identical SNP loci. Use of a paired normal reference also enables allele-based analysis, which can unveil regions of copy neutral LOH in cancer cells. However, allele-based analysis only uses heterozygous SNPs, thus reducing the overall resolution by ~20% compared with the non-allele-based analysis. Recently, large regions with successive homozygous SNPs are reportedly commonly seen in leukemia samples (25).

Figure 2*C* illustrates that when a paired normal reference is unavailable, a best-fit reference can be used, resulting in SD reduction to 0.18 ± 0.03, which is only slightly higher than those obtained using a paired normal reference. In addition, the existence of copy neutral LOH can be also predicted from an unusually long tract of homozygous SNP calls in tumor samples (Fig. 5, *bottom*). Thus, when available, a paired normal reference is the ideal reference, but the average of the best-fit references is an excellent alternative that works satisfactorily in most cases, and at a lower cost.

The advantage of the copy number analysis using GeneChip Mapping 100K arrays over conventional BAC-array CGH lies in its extremely high resolution and availability of genotype information, enabling high-density LOH analysis. Although the number of BAC clones on a single array can vary from ~3,000 to ~32,000, there exists a clear limitation to their resolution because small deletions or gains relative to the size of the average BAC clones can easily escape detection in CGH analysis (Fig. 4*B*). Additional limitations include (*a*) requirement of large amounts of BAC genomic DNA for generating spotted arrays, a process which is difficult to quality control, and (*b*) lack of additional genotyping information indispensable for LOH detections. All of these challenges are overcome by Affymetrix GeneChip Mapping 100K arrays. These arrays are manufactured under stringent quality control procedures; the assay requires only 250 ng of starting genomic DNA per array and provides genotyping information at >99.5% accuracy. Together, these features comprise a comprehensive approach for copy number assessment at a resolution currently not achievable by other means.

This system also has limitations. For instance, polymorphism of primer locus or restriction site would affect the signal intensity that leads to misjudge of copy numbers. Although we can exclude these artifacts when these changes strides over different restriction fragments, validations using other methods are required to validate changes that are confined in a single fragment. It is sometimes difficult to distinguish deletions from large-scale copy number polymorphisms when best-fit references are used. In analyzing disease samples mixed with normal tissues, the amplitude of copy number changes diminishes according to the rate of normal fraction contamination. Whereas extensive SNP selection of the Mapping 100K arrays using >300 individuals likely resulted in the exclusion of SNPs on fragments with restriction site polymorphisms (via Hardy-Weinberg disequilibrium), we cannot exclude the possibility that rare mutations in restriction enzyme sites might affect amplification of affected fragments. Even if this did occur, it is highly unlikely to result in an erroneous copy number estimation because of the low likelihood that the mutation would affect more than one or two adjacent genomic fragments.

In conclusion, our improved copy number detection algorithm, combined with Affymetrix GeneChip Mapping 100K arrays, provides a powerful tool for high-resolution analysis of copy number alterations or variations across the human genome.

Acknowledgments

Received 2/14/2005; revised 4/11/2005; accepted 4/29/2005.

Grant support: Grants-in-Aid from Core Research for Evolutional Science and Technology of Japan Science and Technology Corporation; Research on Human Genome, Tissue Engineering, Ministry of Health, Labour, and Welfare; and Japan Health Science Foundation.

The costs of publication of this article were defrayed in part by the payment of page charges. This article must therefore be hereby marked *advertisement* in accordance with 18 U.S.C. Section 1734 solely to indicate this fact.

References

1. Albertson DG, Ylstra B, Segraves R, et al. Quantitative mapping of amplicon structure by array CGH identifies CYP24 as a candidate oncogene. Nat Genet 2000;25:144–6.
2. Hodgson G, Hager JH, Volik S, et al. Genome scanning with array CGH delineates regional alterations in mouse islet carcinomas. Nat Genet 2001; 29:459–64.
3. Pollack JR, Sorlie T, Perou CM, et al. Microarray analysis reveals a major direct role of DNA copy number alteration in the transcriptional program of human breast tumors. Proc Natl Acad Sci U S A 2002; 99:12963–8.
4. Iafrate AJ, Feuk L, Rivera MN, et al. Detection of large-scale variation in the human genome. Nat Genet 2004; 36:949–51.
5. Sebat J, Lakshmi B, Troge J, et al. Large-scale copy number polymorphism in the human genome. Science 2004;305:525–8.
6. Kallioniemi A, Kallioniemi OP, Sudar D, et al. Comparative genomic hybridization for molecular cytogenetic analysis of solid tumors. Science 1992;258: 818–21.
7. Ishkanian AS, Malloff CA, Watson SK, et al. A tiling resolution DNA microarray with complete coverage of the human genome. Nat Genet 2004;36: 299–303.
8. Bignell GR, Huang J, Greshock J, et al. High-resolution analysis of DNA copy number using oligonucleotide microarrays. Genome Res 2004;14:287–95.
9. Huang J, Wei W, Zhang J, et al. Whole genome DNA copy number changes identified by high density oligonucleotide arrays. Hum Genomics 2004; 4:287–99.
10. Janne PA, Li C, Zhao X, et al. High-resolution single-nucleotide polymorphism array and clustering analysis of loss of heterozygosity in human lung cancer cell lines. Oncogene 2004;23:2716–26.
11. Lieberfarb ME, Lin M, Lechpammer M, et al. Genome-wide loss of heterozygosity analysis from laser capture microdissected prostate cancer using single nucleotide polymorphic allele (SNP) arrays and a novel bioinformatics platform dChipSNP. Cancer Res 2003;63:4781–5.
12. Rauch A, Ruschendorf F, Huang J, et al. Molecular karyotyping using an SNP array for genomewide genotyping. J Med Genet 2004;41:916–22.
13. Wong KK, Tsang YT, Shen J, et al. Allelic imbalance analysis by high-density single-nucleotide polymorphic allele (SNP) array with whole genome amplified DNA. Nucleic Acids Res 2004;32:e69.
14. Zhao X, Li C, Paez JG, et al. An integrated view of copy number and allelic alterations in the cancer genome using single nucleotide polymorphism arrays. Cancer Res 2004;64:3060–71.
15. Zhou X, Cole SW, Hu S, Wong DT. Detection of DNA copy number abnormality by microarray expression analysis. Hum Genet 2004;114:464–7.
16. Fodor SP, Read JL, Pirrung MC, Stryer L, Lu AT, Solas D. Light-directed, spatially addressable parallel chemical synthesis. Science 1991;251:767–73.
17. Pease AC, Solas D, Sullivan EJ, Cronin MT, Holmes CP, Fodor SP. Light-generated oligonucleotide arrays for rapid DNA sequence analysis. Proc Natl Acad Sci U S A 1994;91:5022–6.
18. Kennedy GC, Matsuzaki H, Dong S, et al. Large-scale genotyping of complex DNA. Nat Biotechnol 2003;21:1233–7.
19. Matsuzaki H, Dong S, Loi H, et al. Genotyping over 100,000 SNPs on a pair of oligonucleotide arrays. Nat Methods 2004;1:109–11.
20. Lin M, Wei LJ, Sellers WR, Lieberfarb M, Wong WH, Li C. dChipSNP: significance curve and clustering of SNP-array-based loss-of-heterozygosity data. Bioinformatics 2004;20:1233–40.
21. Rakesh Dugad, Desai UB. A tutorial on Hidden Markov Models. No. SPANN-96.1, 1996. p. 1–16.
22. Rajagopalan H, Lengauer C. Aneuploidy and cancer. Nature 2004;432:338–41.
23. Hans GD. The leukemia-lymphoma cell line facts book. London: Academic Press; 2001. p. 371–2.
24. Carvalho B, Ouwerkerk E, Meijer GA, Ylstra B. High resolution microarray comparative genomic hybridisation analysis using spotted oligonucleotides. J Clin Pathol 2004;57:644–6.
25. Raghavan M, Lillington DM, Skoulakis S, et al. Genome-wide single nucleotide polymorphism analysis reveals frequent partial uniparental disomy due to somatic recombination in acute myeloid leukemias. Cancer Res 2005;65:375–8.

Available online at www.sciencedirect.com
SCIENCE DIRECT®
ELSEVIER
Biochemical and Biophysical Research Communications 347 (2006) 517–526
BBRC
www.elsevier.com/locate/ybbrc

TEL/ETV6 induces apoptosis in 32D cells through p53-dependent pathways

Tetsuya Yamagata, Kazuhiro Maki, Kazuo Waga, Kinuko Mitani *

Department of Hematology, Dokkyo Medical University School of Medicine, Tochigi 321-0293, Japan

Received 20 June 2006
Available online 30 June 2006

Abstract

TEL is an ETS family transcription factor that is critical for maintaining hematopoietic stem cells in adult bone marrow. To investigate the roles of TEL in myeloid proliferation and differentiation, we introduced *TEL* cDNA into mouse myeloid 32Dcl3 cells. Overexpression of TEL repressed interleukin-3-dependent proliferation through blocking cell cycle progression. Also, the presence of TEL triggered apoptosis through the mitochondrial intrinsic pathway on exposure to granulocyte colony-stimulating factor. We found an increase in p53 protein and its DNA binding in the TEL-overexpressing cells. Forced expression of TEL stimulated transcription via the p53-responsive element and increased the expression of cellular target genes for p53 such as cell cycle regulator *p21* and apoptosis inducer *Puma*. Consistently, induction of apoptosis was delayed by pifithrin-α treatment and completely blocked by increased expression of Bcl-2 in the TEL-overexpressing cells. These data collectively suggest that TEL exerts a tumor suppressive function through augmenting the p53 pathway and facilitates normal development of myelopoiesis.

Keywords: Apoptosis; 32D; ETS; Granulocyte colony-stimulating factor; Mitochondria; p21; p53; Pifithrin-α; Puma; TEL; Transcription factor

The *TEL* gene, mapped at 12p13, was originally cloned as a fusion partner for the *platelet-derived growth factor receptor β* gene in the t(5;12)(q33;p13) translocation that was found in chronic myelomonocytic leukemia [1]. TEL is a member of the ETS family of transcription factors that acts as a transcriptional repressor [2,3]. The helix–loop–helix (HLH) domain at the N-terminus is necessary for homodimerization [4] and heterodimerization with other ETS family members such as FLI-1 [5] and TEL2 [6]. The ETS domain at the C-terminus is responsible for DNA binding to the ETS-binding consensus site (EBS) that contains a purine-rich GGAA/T core motif [2]. TEL is known to associate with mSin3A and N-CoR through the HLH and central repression (amino acids 268–303) domains, respectively [7]. TEL is reported to bind directly to histone deacetylase (HDAC)-3 through its internal domain, which is located between the HLH and ETS domains. Through interacting with HDAC, directly or indirectly, TEL is believed to mediate transcriptional repression of genes such as *FLI-1* [2], *Id1* [8], *stromelysin-1* [9], and *Bcl-X_L* [10]. TEL's transcriptional modulator capacity is negatively regulated through phosphorylation on specific serine residues by mitogen-activated protein kinase family member p38 and ERK [11,12].

TEL is widely expressed in embryonic and adult tissues. TEL is dispensable for fetal hematopoiesis in the yolk sac and the liver, but is critical for post-natal hematopoiesis in the bone marrow [13,14]. Moreover, a recent conditional knock-out study demonstrated that TEL plays a role in maintaining hematopoietic stem cells in adult bone marrow [15]. For lineage-specific differentiation, TEL accelerates erythroid but represses megakaryocytic differentiation [16,17]. TEL's *in vitro* function in the myeloid lineage has not yet been reported. Besides its function as a hematopoietic regulator, TEL is reported to have a tumor suppressor function. Overexpression of TEL in Ras-transformed

* Corresponding author. Fax: +81 282 86 5630.
E-mail address: kinukom-tky@umin.ac.jp (K. Mitani).

0006-291X/$ - see front matter © 2006 Elsevier Inc. All rights reserved.
doi:10.1016/j.bbrc.2006.06.127

NIH3T3 cells inhibits cell growth in liquid and soft agar cultures, and suppresses tumor formation in nude mice [9,18].

To investigate whether TEL plays a role in proliferation and/or differentiation of myeloid progenitors, we used 32Dcl3 cells that proliferate in the presence of interleukin-3 (IL-3) and differentiate along the myeloid lineage on granulocyte colony-stimulating factor (G-CSF) treatment [19]. Overexpression of TEL in 32Dcl3 cells impaired IL-3-driven cell proliferation and caused apoptosis on G-CSF treatment. We observed strong induction of p53 protein and augmentation of its downstream targets. We also showed that inhibition of the p53 pathway blocks TEL-induced cell death. These data indicate that TEL works upstream of p53 and stimulates apoptosis of immature myeloid cells.

Materials and methods

Plasmid construction. The expression plasmids pME18S-FLAG-TEL, pCXN2-FLAG-TEL, and pCXN2-FLAG-ΔHLH-TEL [16], and the reporter plasmids WT-2xRGC-Luc and MT-2xRGC-Luc [20,21] have been described previously. TheΔETS-TEL fragment from pME18S-FLAG-ΔETS-TEL [16] was inserted into the *Eco*RI site of pCXN2 to generate pCXN2-FLAG-ΔETS-TEL. The Bcl-2 coding region was excised from pUC-CAGGS-human Bcl2 and introduced into the *Eco*RI site of pCAGIPuro.

Cell culture. Parental 32Dcl3 cells and derivative clones were maintained in RPMI1640 medium supplemented with 10% FCS and 0.25 ng/ml of murine recombinant IL-3 or 10 ng/ml of human recombinant G-CSF (Kirin, Gunma, Japan). Five micrograms per milliliter of cycloheximide (Sigma, St. Louis, MO) was added to the culture to inhibit protein synthesis. The specific p53 inhibitor pifithrin-α (Sigma) was used at a concentration of 0.25 or 1 μM.

Isolation of 32D stable transfectants. To establish stable transfectants overexpressing wild-type TEL, ΔHLH-TEL or ΔETS-TEL, 1×10^7 cells were electroporated with 20 μg cDNA cloned into a pCXN2 plasmid carrying the Neo^R gene at 380 V and 975 μF using a Gene Pulser (BIO-RAD, Hercules, CA). Transfected cells were then selected with 0.8 mg/ml of G418 (Sigma), and limiting dilution was performed to obtain stable clones. The resultant stable clone overexpressing wild-type TEL was further electroporated with 20 μg of pCAGIPuro-Bcl-2 carrying the $puromycin^R$ gene, and selected with 0.5 μg/ml of puromycin (Sigma), and limiting dilution was performed to isolate stable double transfectants.

Northern analysis. To obtain a *p53* probe, a mouse *p53* cDNA fragment of 404 bp was amplified by PCR using a primer set (5′-AACCGCC GACCTATCCTTAC-3′ and 5′-TATGGCGGGAAGTAGACTGG-3′). Northern analysis was performed as described previously [17].

Western analysis. Cells were harvested and lysed in RIPA buffer (20 mM Tris–HCl, pH 8.0, 100 mM NaCl, 0.5% NP-40, 2.5 mM EDTA, 0.8 mM PMSF, and 2000 U/ml Ulinastatin). Western analysis was performed as described previously [12] with primary antibodies against FLAG-tag (Sigma), MDM2, p53, and Bcl-2 (Santa Cruz Biotechnology, Santa Cruz, CA). Bound antibodies were detected using the ProtoBlot AP system (Promega, Madison, WI).

Cell cycle analysis. At indicated time points, 5×10^5 cells were harvested, washed with PBS, fixed, and stained with 50 μg/ml of propidium iodide (PI) at room temperature for 10 min using Cycle TEST™ PLUS (Becton, Dickinson and Company, New Jersey). The DNA content of nuclei was determined with a flow cytometer. Percentages of apoptotic cells were evaluated as the sub-G1 fraction using Cell Quest (Becton–Dickinson and Company).

Annexin V/PI staining. At indicated time points, 5×10^5 cells were harvested, washed with PBS, and then subjected to annexin V/PI staining using an Annexin V/FITC Kit (Bender MedSystems, Vienna). Percentages of apoptotic cells were detected as the annexin V(+)/PI(−) fraction in the flow cytometer and analyzed with CellQuest software.

Assessment of mitochondrial transmembrane potential ($\Delta\Psi_m$). At indicated time points, 5×10^5 cells were harvested, washed with PBS, and incubated with 1 μl/ml of JC-1 and JC-9 dyes using JC-1 and JC-9 Mitochondrial Potential Sensor Kit (Molecular Probe, Eugene, Oregon) at 37 °C for 10 min in the dark. Fluorescence emission shift from red to green was evaluated with a flow cytometer.

EMSA. Electrophoretic mobility shift assay (EMSA) was performed as described previously [16] with [α-^{32}P]dCTP-labeled p53 oligonucleotide (5′-TACAGAACATGTCTAAGCATGCTG-3′). In competition studies, a 100-fold molar excess of unlabeled p53 oligonucleotides (a specific competitor) or mutant p53 oligonucleotides (a non-specific competitor; 5′-TACAGAATCGCTCTAAGCATGCTG-3′) was added to the reaction mixture. Anti-p53 antibody (Santa Cruz Biotechnology) was used for super-shift assay.

Luciferase assay. Exponentially growing parental 32Dcl3 cells were electroporated with 10 μg of the reporter plasmid alone or together with 10 μg of p53 expression plasmid [21], or 5, 10 or 15 μg of TEL expression plasmid (pME18S-FLAG-TEL) filled up with pME18S at 380 V and 970 μF using a Gene Pulser (BIO-RAD). Luciferase assay was performed as described previously [12].

Quantitative RT-PCR analysis. Cells were exposed to G-CSF and total RNA was isolated at times indicated. The genomic DNA was digested before reverse transcription. Specific mRNA was amplified using the SYBER Green amplification system and detected by the ABI Prism 7700 real-time PCR system (Applied Biosystems, CA). The primer sequences are: *p53*: 5′-GTAAACGCTTCGAGATGTTCC-3′ and 5′-GACTGGCC CTTCTTGGTCT-3′, *p21*: 5′-CTGTCTTGCACTCTGGTGTCT-3′ and 5′-GGCACTTCAGGGTTTTCTCT-3′, *Puma*: 5′-GTGACCACTGGCA TTCATTT-3′ and 5′-CCTGACTCCCCATCTTCCT-3′, *BAX*: 5′-ACAG GGGCCTTTTTGCTAC-3′ and 5′-GAGACACTCGCTCAGCTTCTT-3′, *BID*: 5′-GAGATGGACCACAACATCCA-3′ and 5′-AGGCTGTCTT CACCTCATCAA-3′, *BAK*: 5′-TACCTCCACCAGCAGGAAC-3′ and 5′-GACCCACCTGACCCAAGA-3′, and *HPRT*: 5′-CTCTCGAAGTG TTGGATACAG-3′ and 5′-ACAAACGTGATTCAAATCCC-3′.

Results

Overexpression of wild-type TEL in 32Dcl3 cells suppresses cell growth in the presence of IL-3 and provokes rapid cell death on G-CSF treatment

We first examined whether TEL plays any role in myeloid cell proliferation and/or differentiation using the murine IL-3-dependent myeloid cell line 32Dcl3. We established several stable cell lines overexpressing wild-type TEL by transfecting FLAG-tagged TEL expression plasmid (pCXN2-FLAG-TEL). Western analysis with anti-FLAG antibody showed that clones T-1 and T-3 expressed high levels of TEL proteins (Fig. 1A). Two clones transfected with the empty plasmid were used as mock-transfected controls (M-2 and M-3). In parental cells, endogenous TEL proteins were not detected in the Western analysis (data not shown). In the presence of IL-3, the two mock clones showed almost the same rates of cell proliferation and viability as the parental 32Dcl3 cells (data not shown). Notably, the growth rates of the TEL-overexpressing cells were compromised compared with those of the mock cells (Fig. 1B). On withdrawal of IL-3, all clones started to deteriorate and completely lost their viability within 2 days, indicating

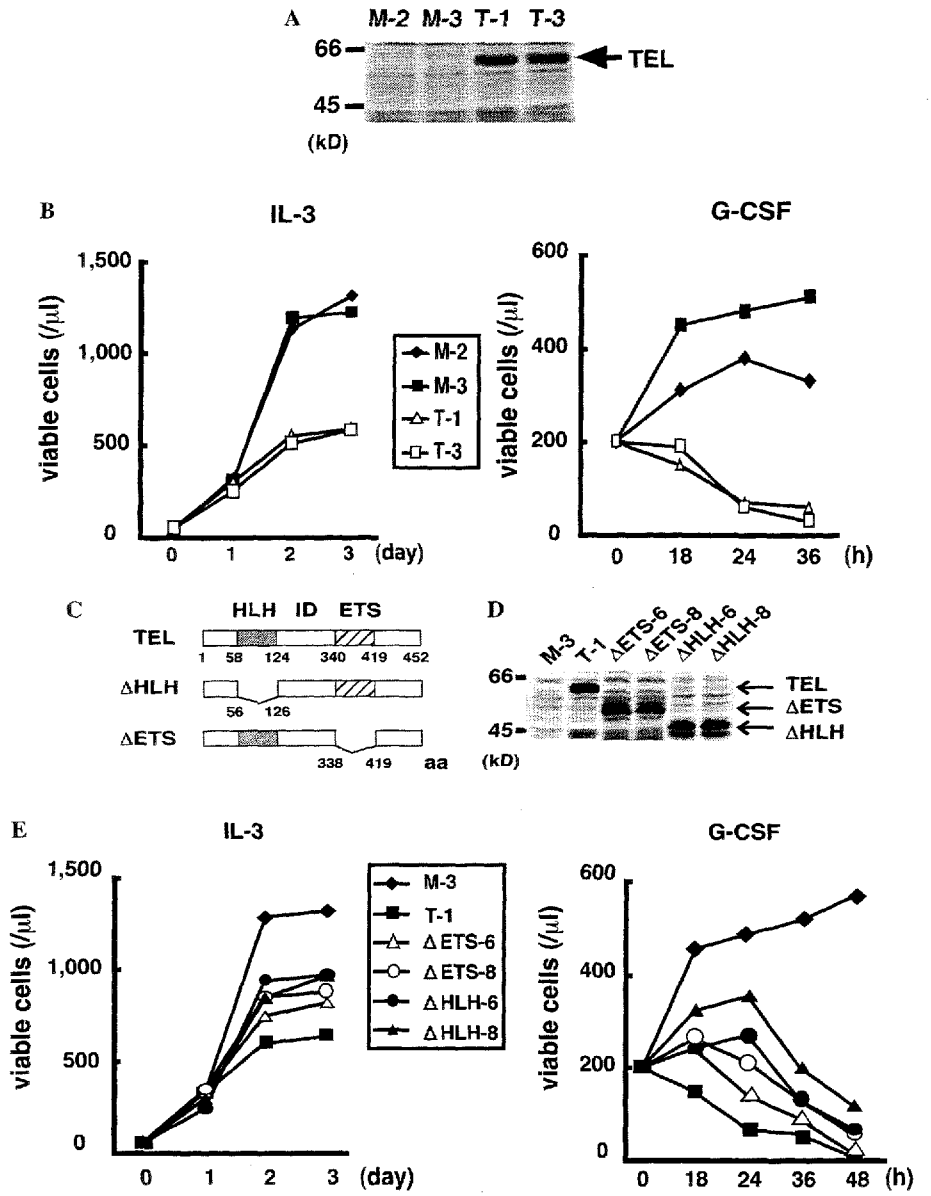

Fig. 1. Overexpression of wild-type TEL causes rapid cell death in 32D cells on G-CSF exposure. (A) Western analysis of 32D clones stably overexpressing wild-type TEL (T-1 and T-3) and mock controls (M-2 and M-3). Arrow indicates overexpressed wild-type TEL detected by anti-FLAG antibody. (B) Time course analysis of viable cell counts in the mock and TEL-overexpressing clones in the presence of IL-3 (in the left panel) or G-CSF (in the right panel). Experiments were repeated three times and reproducible results were obtained. Representative data are shown. (C) Structures of wild-type TEL and the two deletion mutants (ΔHLH-TEL and ΔETS-TEL). The HLH and ETS domains are shown by shaded and hatched boxes, respectively. Numbers indicate amino acids. (D) Western analysis of 32D clones stably overexpressing wild-type TEL (T-1), ΔETS-TEL (ΔETS-6 and ΔETS-8) or ΔHLH-TEL (ΔHLH-6 and ΔHLH-8) and a mock control (M-3) with anti-FLAG antibody. Arrows indicate overexpressed wild-type TEL, ΔETS- and ΔHLH-TEL. (E) Analysis of viable cell counts in M-3, T-1, ΔETS-6, ΔETS-8, ΔHLH-6, and ΔHLH-8 in the presence of IL-3 (in the left panel) or G-CSF (in the right panel). Experiments were repeated three times and similar results were obtained. Representative data are shown.

their dependence on continuous signaling from the IL-3 receptor (data not shown). When IL-3 was replaced with G-CSF, the mock clones underwent differentiation into mature granulocytes, similar to the parental 32Dcl3 cells. In contrast, the TEL-overexpressing clones showed progressive cell death and completely lost their viability within 2 days. We also introduced mutant forms of *TEL* cDNA, *ΔHLH-TEL* and *ΔETS-TEL*, into parental 32Dcl3 cells (Fig. 1C). These cells expressed amounts of the protein similar to those of T-1 (Fig. 1D). The growth rates of the mutant clones were lower than those of the mock cells but higher than those of the wild-type TEL-expressing cells (Fig. 1E). When the ΔHLH-TEL- or ΔETS-TEL-overexpressing cells were treated with G-CSF, their death kinetics fell between those of the mock and wild-type TEL-overexpressing cells. These data suggest that overexpressed TEL suppresses the growth of 32Dcl3 cells in the presence of IL-3 and causes rapid cell death on G-CSF exposure, which partially depend on both the HLH and the ETS domains.

Overexpression of TEL in 32Dcl3 cells stimulates apoptosis on G-CSF treatment

To determine whether this negative effect of wild-type TEL on cell survival after G-CSF treatment is due to induction of apoptosis, we performed DNA content analysis after 12, 24, and 36 h incubation in medium containing G-CSF. Before G-CSF treatment (in the presence of IL-3 only), the G2/M fraction was lower in clones T-1 and T-3 than in clones M-2 and M3 (Fig. 2A), suggesting that TEL has some inhibitory role in cell cycle progression from G0/G1 to the S phase. The occurrence of apoptosis was unlikely in T-1 and T-3 in the presence of IL-3, since we did not observe any increase in the sub-G1 fraction in such conditions. After G-CSF exposure, however, the percentage of the sub-G1 fraction was higher in T-1 and T-3 than in M-2 and M-3 at all the time points examined. Double staining with annexin V and PI was performed to detect early apoptotic cells. Compared with the mock clones, T-1 and T-3 exhibited rapid onset and a higher percentage

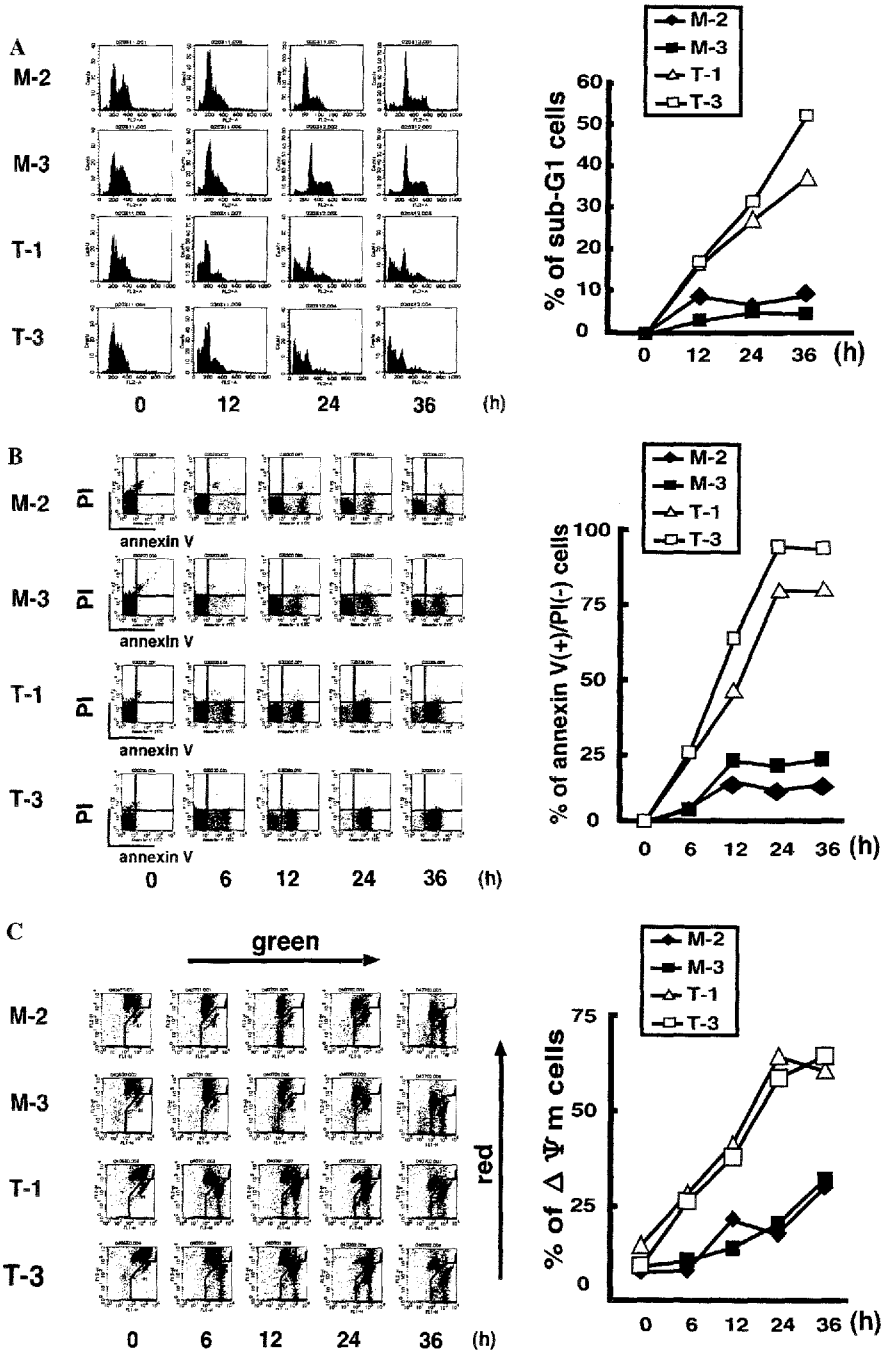

Fig. 2. TEL induces apoptosis in 32D cells under G-CSF treatment. The dead cell fraction was determined using DNA-content analysis (A) or annexin V(+)/PI(−) staining. (B) At indicated time points, cells were stained with PI alone or FITC-conjugated annexin V(+) PI and analyzed in a flow cytometer. (C) TEL-induced apoptosis is associated with loss of mitochondrial membrane potential. At indicated time points, cells were stained with JC-1. Percentages of cells in the lower right fraction were evaluated.

of the early apoptotic fraction (annexin V(+)/ PI(−) quadrant) during G-CSF treatment (Fig. 2B). Thus, TEL enhances apoptotic cell death in 32Dcl3 cells treated with G-CSF.

Wild-type TEL induces apoptosis through mitochondrial depolarization

JC-1 is a cell-permeable cationic dye that selectively accumulates in the polarized mitochondria of live cells but not in the depolarized mitochondria of apoptotic cells [22]. Accumulation of JC-1 in the mitochondria is detected by red fluorescence, which represents aggregation of the dye, while its decomposition, yielding a fluorescence shift from red to green, indicates loss of mitochondrial membrane potential and subsequent apoptosis. Thus, we performed JC-1 staining of the clones in the presence of G-CSF. The ratios of cells showing a shift from red to green after 6-h incubation were much higher in T-1 and T-3 than in the mock cells (Fig. 2C). Thus, overexpression of TEL elicits a drop in the mitochondrial transmembrane potential in G-CSF-treated 32Dcl3 cells. These data indicate that TEL induces apoptosis in 32Dcl3 cells through mitochondrial membrane depolarization.

Overexpression of TEL increases expression of p53

To obtain a molecular insight into the induction of apoptosis, we analyzed the protein levels of Bcl-2 family members. However, expression levels of Bcl-2, Bcl-xL, Bax, Bad, and Noxa were comparable between the mock and TEL-overexpressing cells (data not shown). Surprisingly, we noticed up-regulation of p53 protein [23] in the TEL-overexpressing cells in the presence of either IL-3 or G-CSF (Fig. 3A). The rise in p53 protein level was associated with a small but apparent increase in its mRNA level in both Northern and quantitative PCR analyses (Figs. 3B and 4), suggesting that up-regulation of p53 protein is partly due to an increase of its transcription in TEL-overexpressing cells. This is supported by a rapid decline in

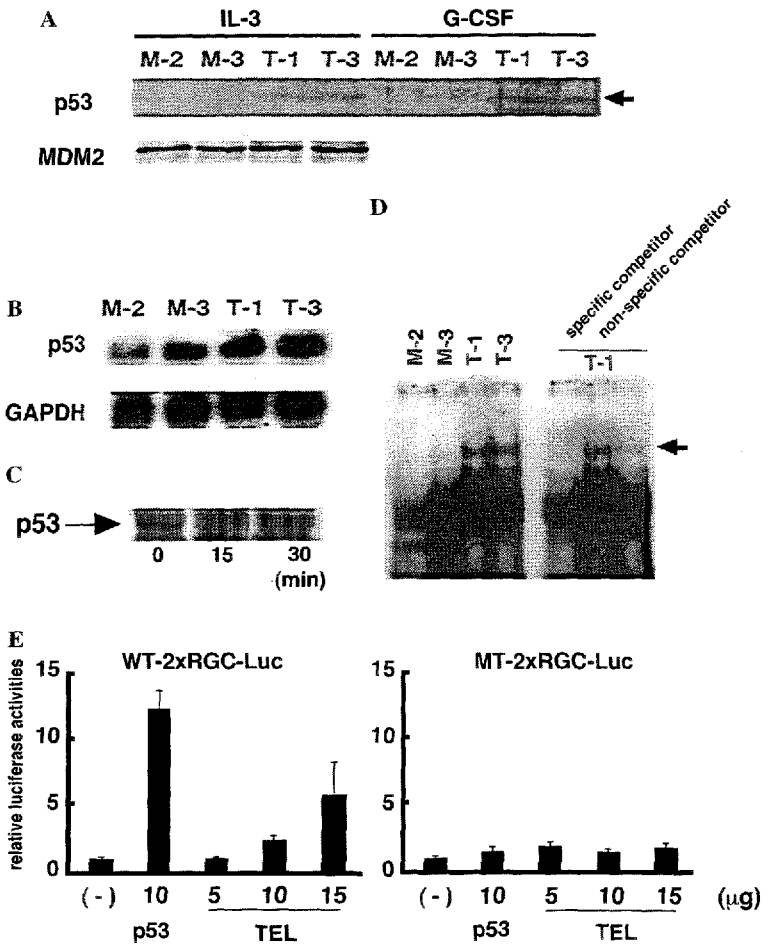

Fig. 3. p53 is up-regulated in TEL-overexpressing cells. (A) Analysis of p53 protein in the mock (M-2 and M-3) and TEL-overexpressing clones (T-1 and T-3) cultured in the presence of IL-3 or G-CSF. Cell lysates were subjected to Western analysis with anti-p53 or anti-MDM2 antibody. (B) Total RNA was subjected to Northern analysis using mouse *p53* cDNA probe. (C) The cells were cultured in the presence of IL-3 with or without 5 μg/ml of cycloheximide for 15 or 30 min. p53 protein was monitored using anti-p53 antibody. (D) EMSA using a specific p53-binding sequence. Arrow indicates specific p53/DNA complex. (E) Parental 32D cells were electroporated with 10 μg of wild-type (WT) or mutated (MT) 2xRGC-Luc reporter plasmid with or without 10 μg of p53 expression plasmid, or 5, 10 or 15 μg of TEL expression plasmid. The results are presented as relative luciferase activity.

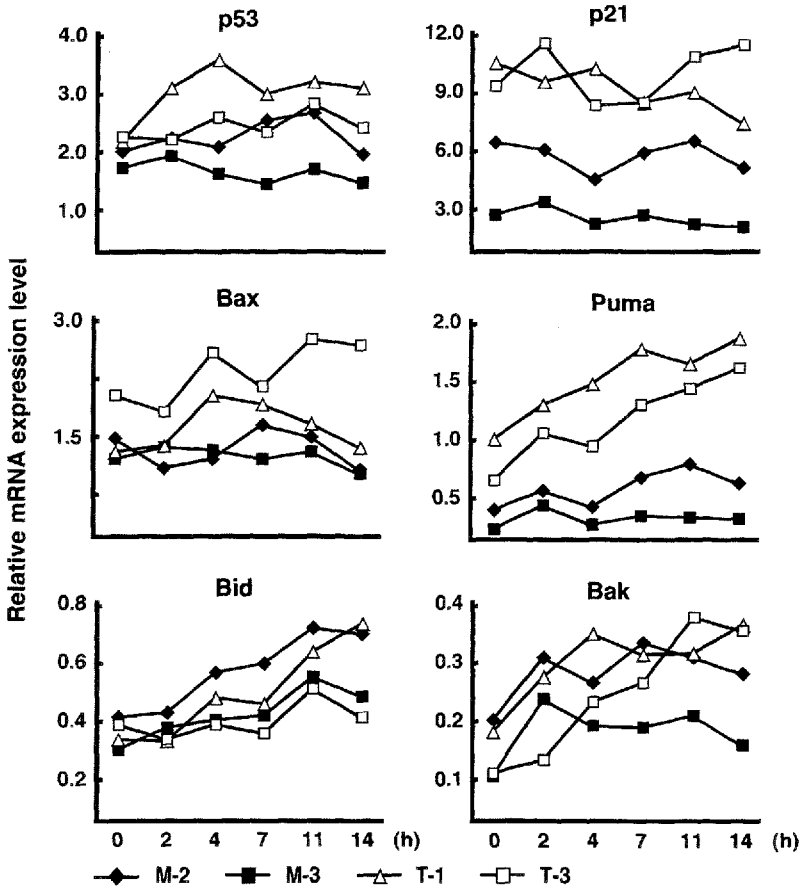

Fig. 4. Genes downstream of p53 are induced in TEL-overexpressing cells. The mock (M-2 and M-3) and TEL-overexpressing (T-1 and T-3) clones were exposed to G-CSF for indicated times and total RNA was isolated. The mRNA of the indicated genes was analyzed by quantitative real-time PCR and normalized against the HPRT mRNA level. BAK is not reported as a p53 target gene.

p53 protein levels after cycloheximide treatment ($T_{1/2}$: less than 7.5 min) (Fig. 3C), which indicates that most of the existing p53 protein is newly synthesized from its mRNA. We also looked at MDM2 protein, which causes ubiquitination and subsequent degradation of p53. Expression of MDM2 protein in the TEL-overexpressing cells was similar to that in the mock transfectants (Fig. 3A). These data suggest that the rise in p53 protein in TEL-overexpressing cells is likely to be due to translation from the increased mRNA rather than stabilization of the protein.

To compare the DNA-binding properties of p53 in the mock and TEL-overexpressing cells, nuclear extracts were prepared from each population and subjected to EMSA using radioactive p53-specific oligonucleotide probe. Consistent with the results of Western analysis, binding of p53 to the specific probe was markedly enhanced in the TEL-overexpressing cells (Fig. 3D). This binding was specific, since the protein–DNA complex was completely canceled by addition of specific cold competitors but not by non-specific competitors. Also, the binding of p53 to the specific probe was canceled by addition of anti-p53 antibody. Thus, overexpression of wild-type TEL results in increased protein levels and subsequent DNA binding of p53. We next investigated whether the increased level of p53 protein would enhance the activity of the p53-dependent reporter plasmid. For this purpose, we chose the WT-2xRGC-Luc reporter, which contains two binding sites for p53, from the ribosomal gene cluster [21]. We transfected WT-2xRGC-Luc together with p53 or wild-type TEL expression plasmid into 32Dcl3 cells and evaluated luciferase activity. Co-transfection of p53 expression plasmid resulted in an approximately 12-fold increase in luciferase activity (Fig. 3E). Interestingly, co-transfection of TEL also activated the reporter in a dose-dependent manner. This activity was completely blocked in reporter plasmid mutated at the p53-binding sites (MT-2xRGC-Luc). This result suggests that potential p53 target genes are activated in wild-type TEL-overexpressing cells.

The p53 target genes are activated in wild-type TEL transfectants

The above results suggest that overexpression of wild-type TEL increases the level of p53 protein, which in turn enhances expression of various p53 target genes involved in cell cycle arrest or apoptosis. To test this hypothesis, we looked at expression levels of p53 target genes in the TEL-overexpressing cells and mock transfectants after

G-CSF treatment. We examined the kinetics of p53 target gene expression after G-CSF exposure, reasoning that the increased level of p53 would elicit a more sensitive response to p53 upstream stimuli, so that the transcription of p53 target genes would increase. Thus, we treated cells with G-CSF and isolated their RNAs at different time points. The expression levels of representative p53 target genes were quantified using real-time PCR. The level of p53 mRNA was higher in the TEL transfectants than in the mock-transfected cells before G-CSF induction (0 h), and this tendency remained throughout the time course (Fig. 4). Thus, the *p53* gene is not induced on G-CSF treatment. Interestingly, the mRNA of p21, the major cell cycle inhibitor downstream of p53, was consistently higher in the TEL-overexpressing cells than in the controls. Also, the mRNA of *Puma*, a pro-apoptotic member of the Bcl-2 family critical for initiation of apoptosis [24], was dramatically induced after G-CSF treatment in the TEL-overexpressing cells. The basal level of *Puma* mRNA was high in T-1 and T-3, but the induction was more significant in these cells than in the controls. Other p53 target genes such as *Bid* and *Bax* showed no significant difference between the TEL-overexpressing and mock-transfected cells. Also, the expression of Bak, a pro-apoptotic gene that is independent of p53, remained the same in the two populations. Thus, induction of *Puma* is likely to be responsible for the death of TEL-expressing cells after G-CSF treatment.

Both transcription-dependent and -independent pathways of p53 contribute to cell death in TEL-expressing cells

The up-regulation of *p21* and *Puma* mRNA in TEL-expressing cells suggests that a transcription-mediated effect of p53 plays a role in G-CSF-triggered apoptosis and growth arrest. To evaluate this further, we treated cells with G-CSF in the presence or absence of pifithrin-α, a chemical compound known to suppress p53-mediated gene transcription [25]. In this experiment, suppression of the p53 target genes would attenuate G-CSF-induced apoptosis in the TEL-expressing cells. In the mock cells, addition of pifithrin-α had no effect on cell survival after G-CSF treatment (Fig. 5A, M-2 and M-3). In the TEL-overexpressing cells, however, pifithrin-α significantly delayed the onset of apoptosis; the cell counts increased at 12 h after G-CSF treatment (T-1: 0 μM vs 0.25 μM, $p = 0.264$; 0 μM vs 1.0 μM, $p = 0.002$; T-3: 0 μM vs 0.25 μM, $p = 0.049$; 0 μM vs 1.0 μM, $p = 0.005$. Student's t, two-tailed, unpaired) followed by a rapid decline after 24–36 h (Fig. 5A, T-1 and T-3). The protective effect of pifithrin-α was dose dependent, with more cells surviving at 12 h at a concentration of 1.0 μM than at 0.25 μM (T-1: 400/μl vs 296/μl; T-3: 383/μl vs 283/μl). Again, no such dosage effect was observed in the mock-transfected cells. These results indicate that induction of the p53 target genes in the TEL-overexpressing cells is at least partly responsible for the induction of apoptosis after G-CSF treatment.

Despite clear inhibition of apoptosis in its early phase by pifithrin-α, cell death still occurs after 24–36 h. It is known that p53 triggers cell death through transcription-independent mechanisms [26]. Physical interaction of mitochondrially translocated p53 with anti-apoptotic Bcl-xL and Bcl-2 is believed to liberate pro-apoptotic BAK from these inhibitors and induce outer membrane permeabilization [27]. Thus, we aimed to block this pathway by overexpression of Bcl-2 to sequester increased p53 protein in the TEL-overexpressing cells and prevent subsequent activation of BAK downstream. Fig. 5B shows the introduction of the Bcl-2 expression plasmid in the TEL-expressing clone T-1 (T-1/B2 and T-1/B5). We also made two stable lines of 32Dcl3 expressing Bcl-2 protein (B-1 and B-2). These

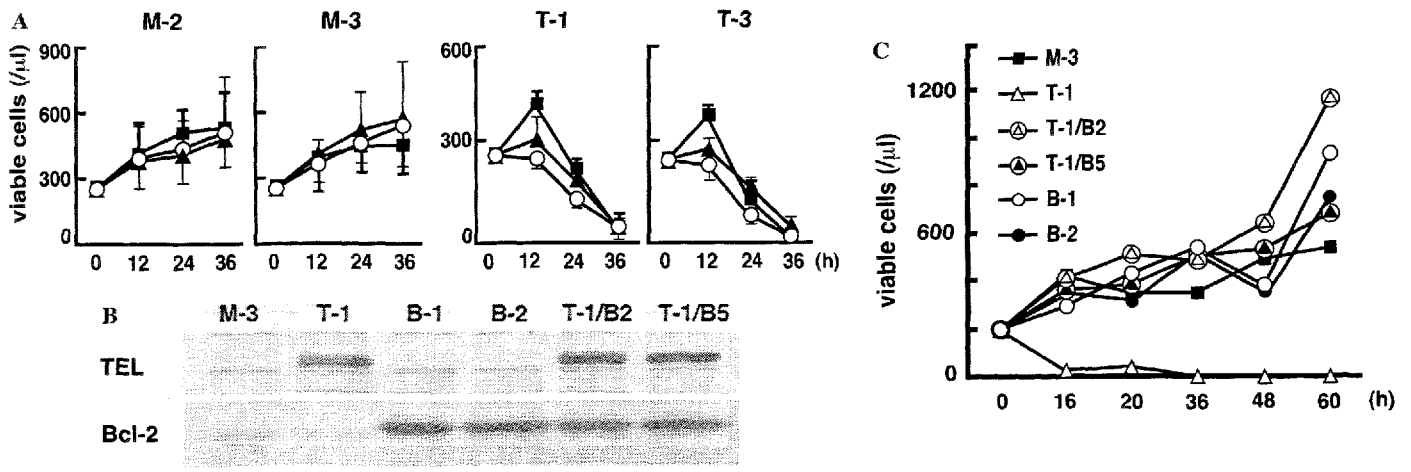

Fig. 5. TEL-induced apoptosis caused by p53 transcription-dependent and -independent mechanisms. (A) The p53 inhibitor pifithrin-α delays the onset of G-CSF-triggered apoptosis in the TEL-expressing cells. The mock (M-2 and M-3) and TEL-overexpressing (T-1 and T-3) clones were cultured in the presence of G-CSF with 0, 0.25 or 1.0 μM of pifithrin-α (shown as ○, ▲, and ■, respectively). Viable cells were counted at the times indicated. The results are shown as averages of three independent experiments, with bars representing standard deviations. (B) Western analysis of 32D clones stably overexpressing wild-type TEL (T-1), Bcl-2 (B-1 and B-2), and both wild-type TEL and Bcl-2 (T-1/B2 and T-1/B5) with anti-FLAG (in the upper panel) or anti-Bcl-2 (in the lower panel) antibody. Bcl-2 expression vector was introduced into parental cells or the TEL-overexpressing clone T-1. (C) Co-expression of Bcl-2 in TEL-overexpressing cells completely suppresses apoptosis. The time courses of viable cells were analyzed after G-CSF treatment.

clones, as well as M-3 and T-1, were treated with G-CSF and the viable cells were counted (Fig. 5C). The Bcl-2 and TEL double transfectants (T-1/B2 and T-1/B5) showed complete resistance to G-CSF-induced apoptosis, indistinguishable from that of Bcl-2 transfectants (B-1 and B-2). Thus, these data indicate that both transcription-dependent and -independent pathways of p53 contribute to cell death in the TEL-expressing cells.

Discussion

We demonstrated in this study that TEL has negative effects on proliferation and survival of 32Dcl3 cells. Wild-type TEL slows the growth of exponentially growing 32Dcl3 cells in the presence of IL-3, apparently as a result of cell cycle arrest. This observation is consistent with its tumor suppressive functions reported in Ras-transformed NIH3T3 cells [9]. In addition, we have found in this study that wild-type TEL rapidly induces apoptosis in 32Dcl3 cells exposed to G-CSF. Since the parental and mock cells differentiate into mature granulocytes on exposure to G-CSF, it is possible that the wild-type TEL-overexpressing cells lose their response to G-CSF stimulation. We examined expression of the G-CSF receptor in the TEL-overexpressing cells; both the mock and the TEL-overexpressing cells expressed similar levels of *G-CSF receptor* transcript, suggesting that loss of cell surface G-CSF receptors is not an underlying mechanism of TEL-induced apoptosis. We also examined the domains necessary for TEL-mediated apoptosis. Deletion of either the HLH or the ETS domain of TEL resulted in partial loss of its apoptosis-induction capacity. This is in contrast with the results of reporter analyses in which deletion of such domains caused complete loss of its function as a transcriptional repressor [16,28]. Thus, at this point it is unclear whether the G-CSF-induced apoptosis is related to TEL's transcriptional function or due to some transcription-independent mechanism. Nevertheless, our observation that TEL-induced apoptosis in the presence of G-CSF suggests its specific role in hematopoietic cells, which may act in synergy with co-existing hematopoietic cytokines.

Apoptosis is initiated following activation of either intrinsic or extrinsic signals. The former are produced by cellular stresses such as exposure to radiation, chemicals, growth factor deprivation, and oxidative stress, while the latter are mediated by crosslinking of the TNF receptor families. In general, intrinsic signals converge on mitochondria, where integration of the cell death machinery takes place [29]. The ratio of pro-apoptotic and anti-apoptotic members of the Bcl-2 family proteins determines how much cellular stress is necessary to initiate apoptosis [30]. Loss of mitochondrial membrane potential detected in the TEL-overexpressing cells suggests that TEL induces apoptosis through the intrinsic pathway. However, we were unable to detect changes in the protein levels of the Bcl-2 family members Bcl-2, Bcl-xL, Bax, Bad, and Noxa, which regulate apoptotic induction through the mitochondria.

Importantly, we observed increased levels of p53 protein in the TEL-overexpressing cells. It has been demonstrated that overexpression of p53 is sufficient to cause apoptosis in several experimental systems [31]. Thus, the higher expression of p53 could cause increased sensitivity to apoptosis once the minimum level of intrinsic death signals is provided. This observation led us to analyze the underlying mechanisms in the increased expression of p53 by wild-type TEL. Cycloheximide treatment for 15 min results in complete disappearance of p53 proteins, indicating that wild-type TEL assists up-regulation of p53 protein primarily through protein synthesis but not through protein stabilization. The finding that MDM2 proteins are expressed at similar levels in mock and TEL-overexpressing cells also supports this idea. Our Northern analysis and real-time PCR assay show that *p53* mRNAs are up-regulated in the TEL-overexpressing cells. Therefore, TEL could contribute in stimulating transcription of the *p53* gene and thereby causing an increase in p53 protein synthesis. The *p53* promoter region contains multiple EBS within 0.5 kb upstream of the translational initiation site [32], though we have not yet obtained evidence that TEL can transactivate the promoter.

The molecular mechanism of TEL's tumor suppressive function has hitherto been a mystery. Our study defined the p53 pathway as one such mechanism. Overexpression of TEL results in increased levels of p53 protein, which are reflected in its increased DNA binding and activation of the p53-responsive reporter. TEL-overexpressing clones show higher expression of p53 target genes such as *p21* and *Puma*, and the induction of apoptosis is blunted by the p53-specific transcription inhibitor pifithrin-α. Overexpression of Bcl-2 completely blocks apoptosis in the TEL-overexpressing clones, indicating that the intrinsic pathway, presumably activated by p53, is responsible for the apoptosis. Collectively, our paper proposes p53 as one of the downstream targets for the tumor suppressive function of TEL.

In human leukemia, the *TEL* gene is frequently translocated to form various fusion genes that generate multiple abnormal chimeric proteins. A proposed mechanism of leukemogenesis by such TEL-fusion proteins is that the HLH domain of TEL assists dimerization of the fusion proteins, thereby eliciting kinase activity intrinsic to the fused partners [1,33–35]. Conversely, generation of the fusion protein could act dominant-negatively to the fused partner, as seen in the case of TEL/AML1 generated as a consequence of t(12;21)(p13;q22) translocation in pre-B cell-type acute lymphoblastic leukemia [36,37]. Some studies suggest that TEL has a tumor suppressive function and that its inactivation could result in formation of the tumor [9]. Our study shows that the anti-oncogenic effect of TEL could be partly attributed to activation of a p53-dependent pathway. Some of the TEL-related fusion proteins have the HLH domain that is necessary for heterodimerization with wild-type TEL. This interaction might inhibit the normal function of wild-type TEL, including induction of p53 pathways,

and thereby assist the development of leukemia. A typical example would be TEL/AML1. We previously reported that TEL/AML1 imposes a dominant-negative effect over wild-type TEL through heterodimerization with the HLH domain [38]. Thus, fusion proteins of TEL that have the TEL–HLH domain may have a similar function to TEL/AML1 and could cause transformation of myeloid progenitors. Such candidate fusion molecules include TEL/ARG in t(1;12)(q25;p13) [39], TEL/ARNT in t(1;12)(q21;p13) [40], and TEL/PTPRR in inv(12)(p13q13) [41]. These proteins may impede the TEL–p53 pathway, which could constitute another mechanism of leukemia development caused by 12p13-related translocations.

Acknowledgments

We thank Dr. J. Miyazaki for pCXN2 and pCAGIPuro, and Dr. Y. Tsujimoto for Bcl-2 cDNA, respectively. IL-3 and G-CSF were kindly provided from KIRIN Brewery Co. Ltd. This work was supported by Grants-in-Aid from the Ministry of Education, Culture, Sports, Science and Technology (Japan), the Ministry of Health, Labour and Welfare (Japan), the Japanese Society for the Promotion of Science, and the Japan Health Sciences Foundation.

References

[1] T.R. Golub, G.F. Barker, M. Lovett, D.G. Gilliland, Fusion of PDGF receptor beta to a novel ets-like gene, tel, in chronic myelomonocytic leukemia with t(5;12) chromosomal translocation, Cell 77 (1994) 307–316.

[2] H. Poirel, C. Oury, C. Carron, E. Duprez, Y. Laabi, A. Tsapis, S.P. Romana, M. Mauchauffe, M. Le Coniat, R. Berger, J. Ghysdael, O.A. Bernard, The TEL gene products: nuclear phosphoproteins with DNA binding properties, Oncogene 14 (1997) 349–357.

[3] R.G. Lopez, C. Carron, C. Oury, P. Gardellin, O. Bernard, J. Ghysdael, TEL is a sequence-specific transcriptional repressor, J. Biol. Chem. 274 (1999) 30132–30138.

[4] C.A. Kim, M.L. Phillips, W. Kim, M. Gingery, H.H. Tran, M.A. Robinson, S. Faham, J.U. Bowie, Polymerization of the SAM domain of TEL in leukemogenesis and transcriptional repression, EMBO J. 20 (2001) 4173–4182.

[5] B.A. Kwiatkowski, L.S. Bastian, T.R. Bauer, J.S. Tsai, A.G. Zielinska-Kwiatkowska, D.D. Hickstein, The ets family member Tel binds to the Fli-1 oncoprotein and inhibits its transcriptional activity, J. Biol. Chem. 273 (1998) 17525–17530.

[6] M.D. Potter, A. Buijs, B. Kreider, L. van Rompaey, G. Grosveld, Identification and characterization of a new human ETS-family transcription factor, TEL2, that is expressed in hematopoietic tissues and can associate with TEL1/ETV6, Blood 95 (2000) 3341–3348.

[7] L. Wang, S.W. Hiebert, TEL contacts multiple co-repressors and specifically associates with histone deacetylase-3, Oncogene 20 (2001) 3716–3725.

[8] R. Martinez, T.R. Golub, Transcriptional repression of ID1 by the leukemogenic ETS protein TEL, Blood 96 (2000) 453a.

[9] R. Fenrick, L. Wang, J. Nip, J.M. Amann, R.J. Rooney, J. Walker-Daniels, H.C. Crawford, D.L. Hulboy, M.S. Kinch, L.M. Matrisian, S.W. Hiebert, TEL, a putative tumor suppressor, modulates cell growth and cell morphology of ras-transformed cells while repressing the transcription of stromelysin-1, Mol. Cell. Biol. 20 (2000) 5828–5839.

[10] B.J. Irvin, L.D. Wood, L. Wang, R. Fenrick, C.G. Sansam, G. Packham, M. Kinch, E. Yang, S.W. Hiebert, TEL, a putative tumor suppressor, induces apoptosis and represses transcription of Bcl-XL, J. Biol. Chem. 278 (2003) 46378–46386.

[11] H. Arai, K. Maki, K. Waga, K. Sasaki, Y. Nakamura, Y. Imai, M. Kurokawa, H. Hirai, K. Mitani, Functional regulation of TEL by p38-induced phosphorylation, Biochem. Biophys. Res. Commun. 299 (2002) 116–125.

[12] K. Maki, H. Arai, K. Waga, K. Sasaki, F. Nakamura, Y. Imai, M. Kurokawa, H. Hirai, K. Mitani, Leukemia-related transcription factor TEL is negatively regulated through extracellular signal-regulated kinase-induced phosphorylation, Mol. Cell. Biol. 24 (2004) 3227–3237.

[13] L.C. Wang, F. Kuo, Y. Fujiwara, D.G. Gilliland, T.R. Golub, S.H. Orkin, Yolk sac angiogenic defect and intra-embryonic apoptosis in mice lacking the Ets-related factor TEL, EMBO J. 16 (1997) 4374–4383.

[14] L.C. Wang, W. Swat, Y. Fujiwara, L. Davidson, J. Visvader, F. Kuo, F.W. Alt, D.G. Gilliland, T.R. Golub, S.H. Orkin, The TEL/ETV6 gene is required specifically for hematopoiesis in the bone marrow, Genes Dev. 12 (1998) 2392–2402.

[15] H. Hock, E. Meade, S. Medeiros, J.W. Schindler, P.J. Valk, Y. Fujiwara, S.H. Orkin, Tel/Etv6 is an essential and selective regulator of adult hematopoietic stem cell survival, Genes Dev. 18 (2004) 2336–2341.

[16] K. Waga, Y. Nakamura, K. Maki, H. Arai, T. Yamagata, K. Sasaki, M. Kurokawa, H. Hirai, K. Mitani, Leukemia-related transcription factor TEL accelerates differentiation of Friend erythroleukemia cells, Oncogene 22 (2003) 59–68.

[17] W. Takahashi, K. Sasaki, N. Komatu, K. Mitani, TEL/ETV6 accelerates erythroid differentiation and inhibits megakaryocytic maturation in a human leukemia cell line UT-7/GM, Cancer Sci. 96 (2005) 340–348.

[18] L.V. Rompaey, M. Potter, C. Adams, G. Grosveld, Tel induces a G1 arrest and suppresses Ras-induced transformation, Oncogene 19 (2000) 5244–5250.

[19] G. Migliaccio, A.R. Migliaccio, B.L. Kreider, G. Rovera, J.W. Adamson, Selection of lineage-restricted cell lines immortalized at different stages of hematopoietic differentiation from the murine cell line 32D, J. Cell. Biol. 109 (1989) 833–841.

[20] S.E. Kern, K.W. Kinzler, A. Bruskin, D. Jarosz, P. Friedman, C. Prives, B. Vogelstein, Identification of p53 as a sequence-specific DNA-binding protein, Science 252 (1991) 1708–1711.

[21] K. Maki, K. Mitani, T. Yamagata, M. Kurokawa, Y. Kanda, Y. Yazaki, H. Hirai, Transcriptional inhibition of p53 by the MLL/MEN chimeric protein found in myeloid leukemia, Blood 93 (1999) 3216–3224.

[22] S. Salvioli, A. Ardizzoni, C. Franceschi, A. Cossarizza, JC-1, but not DiOC6(3) or rhodamine 123, is a reliable fluorescent probe to assess $\Delta\Psi$ changes in intact cells: implications for studies on mitochondrial functionality during apoptosis, FEBS Lett. 411 (1997) 77–82.

[23] S.L. Haris, A.J. Levine, The p53 pathway: positive and negative feedback loops, Oncogene 24 (2005) 2899–2908.

[24] A. Villunger, E.M. Michalak, L. Coultas, F. Mullauer, G. Bock, M.J. Ausserlechner, J.M. Adams, A. Strasser, p53- and drug-induced apoptotic responses mediated by BH3-only proteins puma and noxa, Science 302 (2003) 1036–1038.

[25] P.G. Komarov, E.A. Komarova, R.V. Kondratov, K. Christov-Tselkov, J.S. Coon, M.V. Chernov, A.V. Gudkov, A chemical inhibitor of p53 that protects mice from the side effects of cancer therapy, Science 285 (1999) 1733–1737.

[26] M. Schuler, D.R. Green, Transcription, apoptosis and p53: catch-22, Trends Genet. 21 (2005) 182–187.

[27] M. Mihara, S. Erster, A. Zaika, O. Petrenko, T. Chittenden, P. Pancoska, U.M. Moll, p53 has a direct apoptogenic role at the mitochondria, Mol. Cell 11 (2003) 577–590.

[28] K. Sasaki, Y. Nakamura, K. Maki, K. Waga, F. Nakamura, H. Arai, Y. Imai, H. Hirai, K. Mitani, Functional analysis of a dominant-negative DeltaETS TEL/ETV6 isoform, Biochem. Biophys. Res. Commun. 317 (2004) 1128–1137.

[29] Y. Tujimoto, Cell death regulation by the Bcl-2 protein family in the mitochondria, J. Cell Physiol. 195 (2003) 158–167.
[30] S.J. Korsmeyer, BCL-2 gene family and the regulation of programmed cell death, Cancer Res. 59 (1999) 1693–1700.
[31] E. Yonish-Rouach, D. Resnitzky, J. Lotem, L. Sachs, A. Kimchi, M. Oren, Wild-type p53 induces apoptosis of myeloid leukaemic cells that is inhibited by interleukin-6, Nature 352 (1991) 345–347.
[32] S.P. Tuck, L. Crawford, Characterization of the human p53 gene promoter, Mol. Cell. Biol. 9 (1989) 2163–2172.
[33] M. Eguchi, M. Eguchi-Ishimae, A. Tojo, K. Morishita, K. Suzuki, Y. Sato, S. Kudoh, K. Tanaka, M. Setoyama, F. Nagamura, S. Asano, N. Kamada, Fusion of ETV6 to neurotrophin-3 receptor TRKC in acute myeloid leukemia with t(12;15)(p13;q25), Blood 93 (1999) 1355–1363.
[34] T.R. Golub, A. Goga, G.F. Barker, D.E. Afar, J. McLaughlin, S.K. Bohlander, J.D. Rowley, O.N. Witte, D.G. Gilliland, Oligomerization of the ABL tyrosine kinase by the Ets protein TEL in human leukemia, Mol. Cell. Biol. 16 (1996) 4107–4116.
[35] Y. Kuno, A. Abe, N. Emi, M. Iida, T. Yokozawa, M. Towatari, M. Tanimoto, H. Saito, Constitutive kinase activation of the TEL-Syk fusion gene in myelodysplastic syndrome with t(9;12)(q22;p12), Blood 97 (2001) 1050–1055.
[36] S.W. Hiebert, W. Sun, J.N. Davis, T. Golub, S. Shurtleff, A. Buijs, J.R. Downing, G. Grosveld, M.F. Roussell, D.G. Gilliland, N. Lenny, S. Meyers, The t(12;21) translocation converts AML-1B from an activator to a repressor of transcription, Mol. Cell. Biol. 16 (1996) 1349–1355.
[37] S. Fears, M. Gavin, D.E. Zhang, C. Hetherington, Y. Ben-David, J.D. Rowley, G. Nucifora, Functional characterization of ETV6 and ETV6/CBFA2 in the regulation of the MCSFR proximal promoter, Proc. Natl. Acad. Sci. USA 94 (1997) 1949–1954.
[38] H. Gunji, K. Waga, F. Nakamura, K. Maki, K. Sasaki, Y. Nakamura, K. Mitani, TEL/AML1 shows dominant-negative effects over TEL as well as AML1, Biochem. Biophys. Res. Commun. 322 (2004) 623–630.
[39] Y. Iijima, T. Ito, T. Oikawa, M. Eguchi, M. Eguchi-Ishimae, N. Kamada, K. Kishi, S. Asano, Y. Sakaki, Y. Sato, A new ETV6/TEL partner gene, ARG (ABL-related gene or ABL2), identified in an AML-M3 cell line with a t(1;12)(q25;p13) translocation, Blood 95 (2000) 2126–2131.
[40] F. Salomon-Nguyen, V. Della-Valle, M. Mauchauffe, M. Busson-Le Coniat, J. Ghysdael, R. Berger, O.A. Bernard, The t(1;12)(q21;p13) translocation of human acute myeloblastic leukemia results in a TEL-ARNT fusion, Proc. Natl. Acad. Sci. USA 97 (2000) 6757–6762.
[41] F. Nakamura, Y. Nakamura, K. Maki, Y. Sato, K. Mitani, Cloning and characterization of a novel chimeric gene TEL/PTPRR in acute myelogenous leukemia with inv(12)(p13q13), Cancer Res. 65 (2005) 6612–6621.

Development of megakaryoblastic leukaemia in *Runx1-Evi1* knock-in chimaeric mouse

Leukemia (2006) **20,** 1458–1460. doi:10.1038/sj.leu.2404281; published online 8 June 2006

Chromosomal translocations involving the *Runx1* gene create various chimaeric proteins that are believed to cause human leukaemia. Runx1-ETO and Runx1-Evi1, generated as consequences of t(8;21) and t(3;21), respectively, share molecular structural similarities; they both contain DNA-binding domain of Runx1 and transcriptional repression domains from either ETO or Evi1. Despite such similarity, the subtypes of leukaemia related to each of the chimaeric protein are different; Runx1-ETO typically occurs with acute myelocytic leukaemia of M2 subtype in the French–American–British classification, whereas Runx1-Evi1 is mostly associated with megakaryoblastic leukaemia of M7 subtype or megakaryoblastic crisis in chronic myelocytic leukaemia. Experimental animals that express the fusion proteins in the hematopoietic cells have been created to recapitulate the diseases. Both Runx1-ETO transgenic[1] and conditional knock-in[2] mice do not develop leukaemia by itself and require additional genetic aberrations to transform myeloid progenitors. Here, we report the development of megakaryoblastic leukaemia in *Runx1-Evi1* knock-in chimaeric mouse.

Runx1-Evi1 knock-in chimaeric mice were created by injecting recombinant TT2 ES cells[3] into wild-type blastocyst.[4] We created six of such chimaeric mice, and five of them showed sudden deaths after 7 months of age without any significant finding in post mortem. Interestingly, one of the chimaeric mice that died at 5 months of age showed marked hepatosplenomegaly. Wright–Giemsa staining of stump preparation from the enlarged spleen demonstrated massive infiltration of large dysplastic cells, some of which contained multi-lobulated nuclei with various size of cytoplasm reminiscent of megakaryoblastic leukaemia (Figure 1a). Histology section showed disrupted gross architecture of the spleen, with white and red pulp intermingling (Figure 1c). In the liver, substantial infiltration of leucocytes was observed around the portal vein (Figure 1d). Most of the infiltrating cells consisted of reactive neutrophils, with partial presence of the dysplastic megakaryocytic cells observed in the spleen. Multiple fibrin thrombi were identified in the portal vein, indicating the occurrence of disseminated intravascular coagulation. These findings all

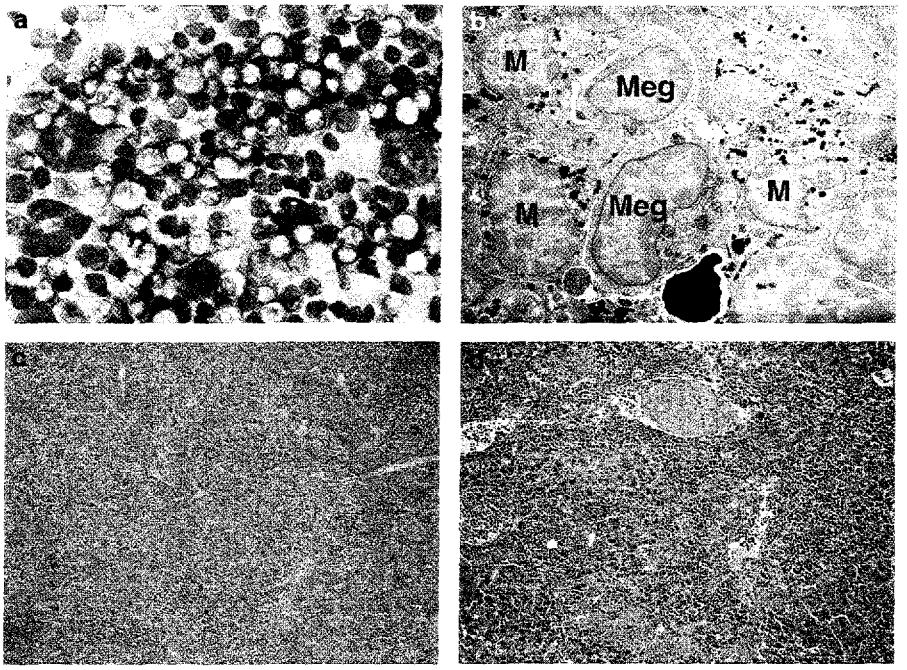

Figure 1 Development of megakaryoblastic leukaemia in *Runx1-Evi1* chimaeric mouse. (**a**) Wright–Giemsa staining of stump preparation from spleen (objective lens (OL), ×40/0.65; original magnification (OM), ×400). (**b**) Electron micrograph of spleen cells (OM, ×3000). M, myeloid cell; Meg, megakaryocytic cell. (**c, d**) Hematoxylin–eosin staining of sections from spleen (**c**) (OL, ×10/0.40; OM, ×100) and liver (**d**) (OL, ×20/0.70; OM, ×200).

indicate an aggressive form of leukaemia. The electron microscopic analysis of the infiltrating cells in the spleen showed 20% of the cells positive for platelet-peroxidase, substantiating megakaryocytic origin of the leukaemic cells (Figure 1b). Taken together, we conclude that this chimaeric mouse developed megakaryoblastic leukaemia.

The key aspect of our observation is that Runx1-Evi1 protein is leukaemogenic *per se*, unlike Runx1-ETO. Such clear difference in the pathophysiological outcome likely arises from the Evi1 portion of Runx1-Evi1 protein. Evi1 is reported to stimulate activator protein 1 activity,[5] repress transforming growth factor-β signaling,[6] and inhibit c-Jun N-terminal kinase function.[7] Such versatile function of Evi1 may underlie stronger oncogenic capacity of Runx1-Evi1 than Runx1-ETO. Another important aspect is that the affected lineage in human is conserved in the experimental animal. Our observation indicates strong causal relationship between the expression of Runx1-Evi1 protein and megakaryoblastic leukaemia. Indeed, the *Runx1-Evi1* chimaeric gene was isolated from a patient developing megakaryoblastic crisis in chronic myelocytic leukaemia that accompanied emergence of *t*(3;21).[8] It is unknown whether Runx1-Evi1 is preferentially oncogenic in megakaryoblast, or show exclusive maturation block in the megakaryocytic lineage when expressed in early haematopoietic cells. Foetal liver cells from *Runx1-Evi1* knock-in heterozygous embryo can give rise to dysplastic megakaryocytes.[4] Such abnormal progenitors may have persisted in the adult bone marrow and expanded to cause massive infiltration of the megakaryoblasts in the liver and spleen.

Acknowledgements

This work was supported by Grants-in-Aid from the Ministries in Japan of Education, Culture, Sports, Science and Technology, and Health, Labour and Welfare, and Japanese Society for the Promotion of Science.

K Maki[1], T Yamagata[1], I Yamazaki[2], H Oda[3] and K Mitani[1]
[1]*Department of Haematology, Dokkyo Medical University School of Medicine, Tochigi, Japan;*
[2]*Department of Clinical Laboratory and Pathology, Inoue Memorial Hospital, Chiba, Japan and*
[3]*Department of Pathology, Tokyo Women's Medical University, Tokyo, Japan*
E-mail: kinukom-tky@umin.ac.jp

References

1 Yuan Y, Zhou L, Miyamoto T, Iwasaki H, Harakawa N, Hetherington CJ *et al.* AML1-ETO expression is directly involved in the development of acute myeloid leukemia in the presence of additional mutations. *Proc Natl Acad Sci USA* 2001; **98**: 10398–10403.
2 Higuchi M, O'Brien D, Kumaravelu P, Lenny N, Yeoh EJ, Downing JR. Expression of a conditional AML1-ETO oncogene bypasses embryonic lethality and establishes a murine model of human t(8;21) acute myeloid leukemia. *Cancer Cell* 2002; **1**: 63–74.
3 Yagi T, Tokunaga T, Furuta Y, Nada S, Yoshida M, Tsukada T *et al.* A novel ES cell line, TT2, with high germline-differentiating potency. *Anal Biochem* 1993; **214**: 70–76.
4 Maki K, Yamagata T, Asai T, Yamazaki I, Oda H, Hirai H *et al.* Dysplastic definitive hematopoiesis in AML1/EVI1 knock-in embryos. *Blood* 2005; **106**: 2147–2155.
5 Tanaka T, Nishida J, Mitani K, Ogawa S, Yazaki Y, Hirai H. Evi-1 raises AP-1 activity and stimulates c-fos promoter transactivation with dependence on the second zinc finger domain. *J Biol Chem* 1994; **269**: 24020–24026.
6 Kurokawa M, Mitani K, Irie K, Matsuyama T, Takahashi T, Chiba S *et al.* The oncoprotein Evi-1 represses TGF-β signalling by inhibiting Smad3. *Nature* 1998; **394**: 92–96.

7 Kurokawa M, Mitani K, Yamagata T, Takahashi T, Izutsu K, Ogawa S *et al.* The evi-1 oncoprotein inhibits c-Jun N-terminal kinase and prevents stress-induced cell death. *EMBO J* 2000; **19**: 2958–2968.

8 Mitani K, Ogawa S, Tanaka T, Miyoshi H, Kurokawa M, Mano H *et al.* Generation of the AML1-EVI-1 fusion gene in the t(3;21)(q26;q22) causes blastic crisis in chronic myelocytic leukemia. *EMBO J* 1994; **13**: 504–510.

The role of the *bax* gene polymorphism G(−248)A in chronic lymphocytic leukemia

Leukemia (2006) **20**, 1460–1461. doi:10.1038/sj.leu.2404280; published online 8 June 2006

Two recent publications in *Leukemia* have investigated the potential role of the *bax* G(−248)A polymorphism in chronic lymphocytic leukemia (CLL),[1,2] which pertain to our previous study,[3] and that of Saxena *et al.*[4] Our single centre study of 203 patients showed that this polymorphism significantly influenced Bax protein expression, overall survival ($P=0.05$) and in particular survival from first treatment ($P=0.012$). In contrast to the original paper by Saxena *et al.*[4] we showed no difference in allele frequency between CLL samples and those derived from healthy volunteers, nor an increased incidence of the polymorphism in advanced stage disease. Unfortunately, Nuckel *et al.*[2] misquote our work by stating that we showed an association between the polymorphism and advanced stage disease — we did not ($P=0.62$). In all other aspects, Nuckel *et al.*[2] assessed clinical and prognostic parameters that we and Skogsberg *et al.*[1] had previously identified as irrelevant with regards to the *bax* G(−248)A polymorphism. Crucially, they failed to address the pivotal question of the role of the polymorphism on therapeutic response.

Although many of the findings from the study of Skogsberg *et al.*[1] (463 patients) and our own are compatible, there are a number of major differences. (1) They failed to identify any significant overall survival difference (median survival 85 months versus 102 months; $P=0.21$ in 350 patients) or survival from first treatment (median survival 36 months versus 63 months; $P=0.26$ in 98 patients). (2) They could not demonstrate a difference in *bax* RNA expression between the polymorphic groups. These differences between the two studies are worthy of further comment.

Our study was a single centre study in which all the clinical data was complete, whereas in the study of Skogsberg *et al.*[1] (a multicentred international collaboration involving seven centres in three countries), there were some significant omissions of clinical data. Survival from treatment data was presented for only 98 patients when their study contains 154 Binet B/C patients. In addition, with a median follow-up of 60 months, a significant number of the 243 stage A patients would also have required therapy and could therefore have been included too. Despite this, their study showed a 27-month difference in survival from therapy between the different polymorphic groups (36 months versus 63 months; $P=0.26$) that is, a trend towards worse survival. We make explicit in our study that virtually all the patients were entered into the prevailing Medical Research Council CLL study at the time. This means that the indications to commence therapy and disease assessment were standardized according to internationally accepted criteria and indeed the therapies the patients received were not too dissimilar – very difficult to control for in a retrospective, multinational, multi-centre study such as Skogsberg *et al.*[1] More disconcerting is how the 98 patient 'subset' were selected? It is clear from Figure 3b that Skogsberg *et al.*[1] chose to look at 73 GG patients who had died. It is clear that for the GA subgroup they chose dead and alive patients. Why did they not just compare the dead GG subgroup with the dead GA subgroup? – this would have at least stopped any, albeit unintentional bias being introduced. How did the authors choose which of the over 60 live GA subgroup to include in this analysis?

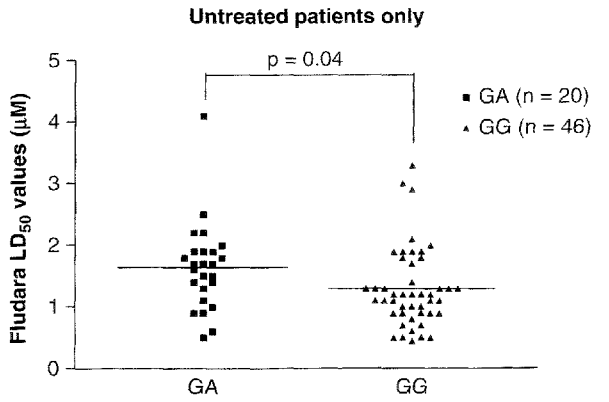

Figure 1 *In vitro* sensitivity (LD_{50}) to fludarabine in 66 previously untreated CLL patients defined by *bax* genotype.

Skogsberg *et al.*[1] stated that they could find no difference in *bax* RNA expression for the different polymorphic groups. However, they only studied 35 patient samples and failed to state how many of these samples were derived from patients who had received prior therapy. This is important as it has been shown that previous treatment exposure is a contributory factor in determining Bax protein expression.[3–5] In our study, we measured Bax protein (122 patients) not RNA and found overlapping, but significantly different Bax expression between the different polymorphic groups. In new data presented here, we show that CLL samples derived from previously untreated patients with the *bax* G(−248)A polymorphism are more resistant to *in vitro* fludarabine (Figure 1). However, the large overlap in fludarabine LD_{50} values between the polymorphic groups indicate that *bax* genotype is not the only determinant of drug sensitivity in CLL cells.

As outlined above, the Skogsberg *et al.*[1] study has several flaws and we look forward to larger prospective studies in CLL and other human malignancies that will hopefully offer definitive evidence of the importance of this single-nucleotide polymorphism in determining treatment response and clinical outcome.

C Fegan[1,4], J Starczynski[2], G Pratt[2,3] and C Pepper[1]
[1]*Department of Haematology, Wales School of Medicine, Cardiff University, Heath Park, Cardiff, UK;*
[2]*Department of Haematology, Heart of England NHS Trust,*

showed the marked growth suppression of MPC-1$^-$ immature myeloma cells, but not MPC-1$^+$ mature myeloma cells in the MM2 case. In the primary myeloma cells from 20 cases, we summarized that the combination of Dex with baicalein showed consistent growth suppression in MPC-1$^-$ immature myeloma cells from all cases, and MPC-1$^+$ mature myeloma cells were significantly suppressed in seven out of 20 cases.

The ligand-induced activation of PPARβ is reported to suppress the NF-κB activity. Two possible mechanisms for its downregulation of NF-κB activity were reported: one was the upregulation of IkB gene expression[7] and the other was the inhibitory physical interaction between the p65 subunit of NF-κB and PPAR in the nucleus.[8] We examined whether PPARβ interacted with the p65 of NF-κB after IL-1α stimulation by the immunoprecipitation followed by Western blotting. Costimulation of IL-1α with Dex and baicalein strongly enhanced the physical interaction between p65 of NF-κB and PPARβ (data not shown). The binding activity of NF-κB (p65/p50) to the κB site was also suppressed in the treatment with Dex and baicalein. Furthermore, the expression of the NF-κB target genes, such as *IL-6* and *IkBα*, was markedly reduced by the treatment of Dex and baicalein combined with IL-1α stimulation in U266 cells.

With regard to the therapeutic aspect, the cooperative growth suppression of Dex and baicalein in myeloma cells might be useful for myeloma therapy. Combinatory treatment with both may overcome the Dex resistance and the baicalein resistance in primary myeloma cells, as well as myeloma cell lines. It is possible that baicalein combined with Dex can induce the activation of PPARβ and glucocorticoid receptor (GR), which cooperatively suppress the transcriptional activity of NF-κB in the nucleus of myeloma cells. Clinical trials would rapidly evaluate the utility of this combinatory treatment in relapsed and refractory myeloma cases.

Acknowledgements

This work was supported in part by grants from the Ministry of Education, Science, Sports and Culture of Japan, the Ministry of Health, Labour and Welfare of Japan; and S Abroun is a recipient of the Postdoctoral Fellowship Award for Foreign Researchers (PO4500) from JSPS.

K-I Otsuyama[1], Z Ma[1], S Abroun[1], J Amin[1], K Shamsasenjan[1], H Asaoku[2] and MM Kawano[1]
[1]*Laboratory of Cellular Signal Analysis, Department of Bio-Signal Analysis, Applied Medical Engineering Science Graduate School of Medicine, Yamaguchi University, Ube, Yamaguchi, Japan and*
[2]*4th Department of Internal Medicine, Hiroshima Red Cross Hospital Hiroshima, Hiroshima, Japan*
E-mail: mkawano@yamaguchi-u.ac.jp

References

1 Dreyer C, Krey G, Keller H, Givel F, Helftenbein G, Wahli W. Control of the peroxisomal beta-oxidation pathway by a novel family of nuclear hormone receptors. *Cell* 1992; **68**: 879–887.
2 Park BH, Vogelstein B, Kinzler KW. Genetic disruption of PPARδ decreases the tumorigenicity of human colon cancer cell. *Proc Natl Acad Sci USA* 2001; **98**: 2598–2603.
3 Bharti AC, Donato N, Singh S, Aggarwal BB. Curcumin (diferuloylmethane) down-regulates the constitutive activation of nuclear factor-kB and IkBα kinase in human multiple myeloma cells, leading to suppression of proliferation and induction of apoptosis. *Blood* 2003; **101**: 1053–1062.
4 He T, Chan TA, Vogelstein B, Kinzler KW. PPARδ is an APC-regulated target of nonsteroidal anti-inflammatory drugs. *Cell* 1999; **99**: 335–345.
5 Ma Z, Otsuyama K, Liu S, Abroun S, Ishikawa H, Tsuyama N *et al.* Baicalein, a component of *Scutellaria* radix from Huang-Lian-Jie-Du-Tang (HLJDT), leads to suppression of proliferation and induction of apoptosis in human myeloma cells. *Blood* 2004; **105**: 3312–3318.
6 Kawano MM, Huang N, Harada H, Harada Y, Sakai A, Tanaka H *et al.* Identification of immature and mature myeloma cells in the bone marrow of human myelomas. *Blood* 1993; **82**: 564–570.
7 Delerive P, Gervois P, Fruchart JC, Staels B. Induction of IkBα expression as a mechanism contributing to the anti-inflammatory activities of peroxisome proliferators-activated receptorα activators. *J Biol Chem* 2000; **275**: 36703–36707.
8 Planavila A, Laguna JC, Vazquez-Carrera M. Nuclear factor-kB activation leads to down-regulation of fatty acid oxidation during cardiac hypertrophy. *J Biol Chem* 2005; **280**: 17464–17471.

Chronic idiopathic myelofibrosis expressing a novel type of *TEL-PDGFRB* chimaera responded to imatinib mesylate therapy

Leukemia (2007) **21**, 190–192. doi:10.1038/sj.leu.2404397; published online 23 November 2006

Constitutive activation of platelet-derived growth factor receptor (PDGFR) is one of the features of myeloproliferative disease (MPD).[1] PDGFR is a member of type III receptor tyrosine kinase that transmits mitotic signals in cells of mesenchymal origin. Both *PDGFRA* and *PDGFRB* genes, located on chromosomes 4q12 and 5q33 respectively, form fusion gene as a result of chromosome translocation. Representative examples are *TEL-PDGFRB* in t(5;12)(q33;p13)[2] and *FIP1L1-PDGFRA* in del(4)(q12),[3] both of the gene products known to have ligand-independent kinase activity. The former is observed in chronic myelomonocytic leukaemia (CMMoL) as well as other MPDs with eosinophilia, whereas the latter has been reported in hypereosinophilic syndrome (HES).

We report here a case of chronic idiopathic myelofibrosis (CIMF) with t(5;12)(q33;p13), which transformed to acute myelogenous leukaemia (AML). This case is unique in two aspects: (1) this is the first report of CIMF with *TEL-PDGFRB* fusion and (2) a novel type of *TEL-PDGFRB* fusion transcript that retained the internal and ETS domains of TEL was expressed. The leukaemic cells responded well to a series of chemotherapy, which was followed by administration of imatinib mesylate, a kinase inhibitor for both PDGFR and ABL. It gave a partial cytogenetic response but failed to maintain a remission of leukaemia. This case implies the existence of various types of *TEL-PDGFRB* fusion gene with possible impact on the phenotype of the disease.

A 37-year-old male presented with nasal and gingival bleeding in August 2005. He showed marked hepatosplenomegaly at presentation: spleen was palpable 10 cm below the left

costal margin, and liver 2 cm below the right costal margin. Laboratory examination revealed a haemoglobin level of 7.6 g/dl, a white blood cell count of 2.8×10^9/l (13.5% blasts) and a platelet count of 9.0×10^9/l. Six per cent erythroblasts as well as dacryocytes were observed in the peripheral blood. The bone marrow could hardly be aspirated. Histological examination of the biopsied specimen showed marked myelofibrosis accompanied by focal proliferation of blast-like cells and megakaryocytes among reticulin fibres. The blastic cells in the peripheral blood were negative for myeloperoxidase, nonspecific esterase, CD13 and CD41, but positive for CD33 (94.2%), CD34 (78.8%), CD56 (92.1%) and HLA-DR (88.4%). Because neither lymphoid markers nor electron microscopic platelet peroxidase activities were detected in the leukaemic cells, he was diagnosed as AML M0 according to the FAB classification. The preceding history of slight leukocytosis (15.6×10^9/l) at 16 months before the diagnosis and the presence of severe myelofibrosis with massive splenomegaly and tear drop cells at presentation suggested that his leukaemia had been transformed from CIMF. Cytogenetic analysis of the peripheral blood cells showed abnormality of 46, XY, t(5;12)(q33;p13)[2]/46, idem, −17, +r1[17]/47, idem, +8, −17, +r1[1]. The patient was treated with induction course of chemotherapy consisting of cytarabine and idarubicin. After one course of chemotherapy, complete remission was achieved morphologically with improvement of myelofibrosis and recovery of platelet count. Additional two courses of chemotherapy with high-dose cytarabine for consolidation maintained morphological remission. Although cells with normal karyotype transiently appeared in the bone marrow during these courses of chemotherapy, the stem line clone carrying t(5;12) never disappeared and formed 100% of the dividing cells at the end of the consolidation therapy. Imatinib mesylate treatment (400 mg/day) was commenced in November 2005 and continued for 3 months until February 2006 when anaemia and leukocytopenia emerged accompanied by high fever and unconsciousness. Serum calcium and C-reactive protein levels increased up to 13.8 and 14.43 mg/dl, respectively. Bone scintigraphy showed abnormal uptakes in multiple regions such as right shoulder and left femur, suggesting the relapse of AML with multiple blastoma in the bone. Although the bone marrow aspirate became dry again, chromosome analysis revealed re-emergence of normal clone but also the sidelines with the same additional abnormalities as those seen at presentation. Despite the intensive chemotherapy with cytarabine and idarubicin, leukaemic cells reappeared in the peripheral blood. The patient succumbed to multiple organ failure owing to disseminated intravascular coagulation syndrome and died in March 2006 (Figure 1).

Based on the physical and laboratory findings, and the clinical course, this patient was diagnosed as AML transformed from CIMF. No t(5;12)(q33;p13) has been reported in CIMF cases so far. Nested reverse transcription-PCR experiment of the peripheral blood specimen at diagnosis using HemaVision leukaemia typing/subtyping system (DNA Technology A/S, Aarhus, Denmark) showed single *TEL-PDGFRB* fusion product that was larger in size than expected. Sequencing analysis of the product revealed in-frame fusion between exon 7 of *TEL* gene and exon 10 of *PDGFRB* gene (*TEL7-PDGFRB10*; Figure 2). All other common leukaemogenic fusion genes screened by HemaVision including major *BCR-ABL* were not detected. $JAK2^{V617F}$, frequently found in MPDs including CIMF, was not detected in this case.

In all previously reported cases with the t(5;12)(q33;p13) translocation, exon 4 of *TEL* gene was fused in-frame to exon 11 of *PDGFRB* gene (2) (*TEL4-PDGFRB11*). TEL4-PDGFRβ11 consists of the sterile-alpha-motif (SAM) domain of TEL, which fuses to the transmembrane and catalytic domains of PDGFRβ. The SAM domain of TEL is known to act as the interface for

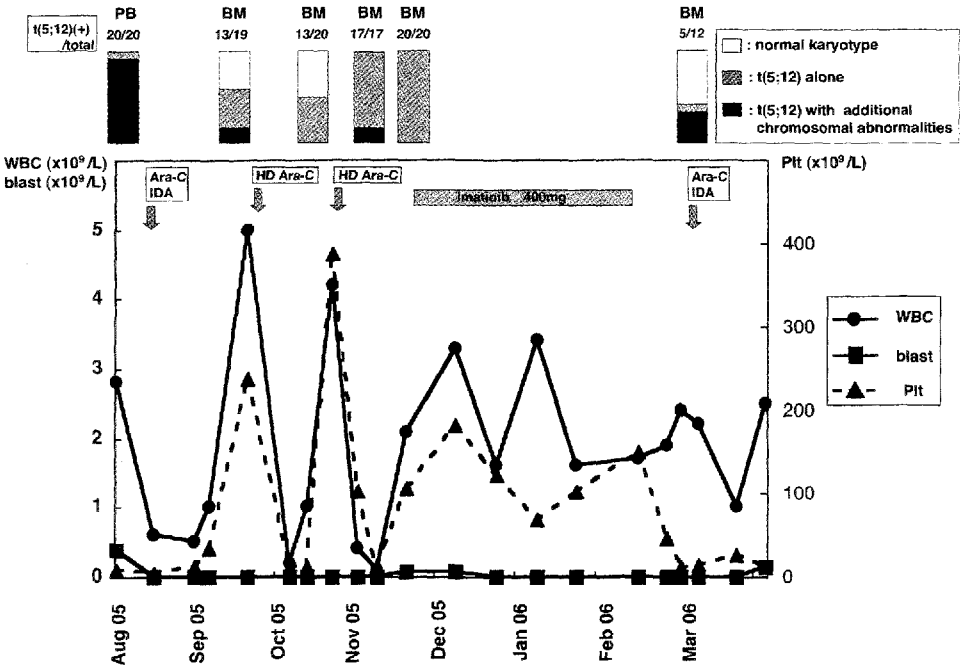

Figure 1 Clinical course. Imatinib was commenced in November 2005 following 3 courses of chemotherapy. At this point, although complete remission of acute leukaemia was achieved morphologically, all dividing cells analysed cytogenetically had t(5;12). After 3 months of imatinib therapy, partial cytogenetic response was obtained with the appearance of cells having normal karyotype. Boxes in the top represent the results of cytogenetic analysis and numbers indicate the ratio of the t(5;12)-positive cells in the total. Abbreviations: PB, peripheral blood; BM, bone marrow; HD, high dose; Ara-C, cytarabine; IDA, idarubicin; WBC, white blood cell; Plt, platelet.